ASSESSMENT OF SOIL PROPERTIES IN PROXIMITY TO ABANDONED OIL WELLS USING REMOTE SENSING AND CLAY X-RAY ANALYSIS, WOOD COUNTY, OHIO

Matthew James Magdic

A Thesis

Submitted to the Graduate College of Bowling Green
State University in partial fulfillment of
the requirements for the degree of

MASTER OF SCIENCE

August 2016

Committee:

Anita Simic, Advisor

Jeff Snyder

John Farver

ABSTRACT

Anita Simic, Advisor

The oil and gas booms of the late 19th century left tens of thousands of wells in Wood County, Ohio abandoned and improperly capped. This allows hydrocarbons to seep into the surrounding soil. Detection of these wells proves difficult because many of the wells are buried and their locations lost. To be able to detect the oil wells over large areas, different remote sensing techniques can be used to detect changes in soil properties caused by the presence of hydrocarbons. However, the capability of this technology depends on spatial and spectral resolution of a sensor and in situ data are often necessary. In this study, in-situ hyperspectral reflectance data and thermal imaging are used in conjunction with clay mineral X-ray diffraction analysis to identify soil properties around abandoned wells located in an agricultural area in Wood County, Ohio. This study is confirmation of previous finding and it serves to indicate uncertainties related to a limited sampling effort, and to address the importance of field sampling strategies and adequate remote sensing techniques. Non-commercial satellite based remote sensors of medium, spatial resolution, such as Landsat, are inadequate for detection of the small abandoned wells in Wood County, Ohio. In situ hyperspectral reflectance measurements, used to simulate WorldView-3 spectral and spatial resolution, suggest that this high spatial resolution commercial satellite is optimal for detecting small abandoned oil wells. It is confirmed that a spectral band ratio in the spectral range between 2.185-2.225 μm and 2.295-2.365 μm (WorldView-3 shortwave bands 6 and 8, respectively) is effective. The clay mineral X-ray diffraction analysis suggests that these changes in the spectral information occur predominately due to the hydrocarbons; clay mineral content changes in the soil did not affect the soil spectral

signature to a greater extent. Thermal imaging identified higher surface temperatures in soil with higher hydrocarbon content when compared to a control site. Based on direct hydrocarbon testing results, only long chain hydrocarbons (C30+) are present in the soil, suggesting that the wells are not active and that hydrocarbons are not presently leaking from the well. Rather, the soil contamination originated in the past, most likely during drilling of the wells decades ago. The limited results in this study are suggestive for further research. More field data, including crop information are needed to support the effectiveness of remote sensing technology in similar studies. It is suggested that using high spectral resolution commercial satellites (e.g. WorldView-3) in conjunction with thermal imaging can be an optimal approach to identify the soil contamination in proximity to abandoned wells in Wood County, Ohio.

ACKNOWLEDGMENTS

I would like to thank all the people who helped with this project. First, I want to thank my advisor Dr. Anita Simic for her guidance, encouragement, and occasional prodding. Without her this project would not have happened. Also, I want to thank my committee members, Dr. Jeff Snyder and Dr. John Farver, for their support and their constructive criticism. Furthermore, I would like to thank the Geology Department at Bowling Green State University for their support. Funding for this project was provided thanks to the Richard C. Fox Practical Geophysics Award.

Lastly, I would like to thank my parents and family for their encouragement and support in my studies and research, without which this project would never have been completed.

TABLE OF CONTENTS

LIST OF FIGURES

LIST OF TABLES

LIST OF TERMS

Term	Acronym
Advanced Spaceborne Thermal Emission and Reflectance Radiometer	ASTER
Advanced Very High Resolution Radiometer	AVHRR
Diesel Range Organics	DRO
Enhanced Thematic Mapper	ETM+
Fast Line-of-sight Atmospheric Analysis of Spectral Hypercubes	FLAASH
Figure of Merit	FOM
Gasoline Range Organics	GRO
Moderate Resolution Imaging Spectroradiometer	MODIS
Near Infrared	NIR
Ohio Department of Natural Resources	ODNR
Oil Range Organics	ORO
Reference Intensity Ratio	RIR
Satellite Pour l'Observation de la Terre Vegetation	SPOT VGT
Short Wave Infrared	SWIR
Thermal infrared	TIR
Thematic Mapper	TM
Visual	VIS
Visual/Near Infrared	VNIR
X-ray Diffraction	XRD

INTRODUCTION

When the oil boom occurred in Northwest Ohio in the late 19th century, tens of thousands of wells were drilled throughout the area in an attempt to extract the abundant oil. After the boom ended, many of the abandoned wells, in an attempt to be capped, were filled with rocks and tree stumps. This improper sealing of the wells commonly allows oil and gas to percolate up to the surface. As recently as 2012, seepage of natural gas and oil occurred in several locations from abandoned wells near Bowling Green, Ohio (Ryan, 2012; Espen, pers. comm.). Of the approximately 36,000 abandoned oil wells believed to be in Wood County, the locations of only about 6,000 are known (Espen, pers. comm.).

Today, many of these wells are part of agricultural fields where oil can negatively impact both soil and crops. Farmers often neglect to report abandoned wells and they are small and hard to detect otherwise (Espen, pers. comm.). Well casings are often cut off below the surface and buried to prevent them from interfering with farming equipment, which further inhibits their detection (NEOGAP, 2009). In addition to soil contamination, these wells are a source of contamination for underground water aquifers that are used for drinking water (NEOGAP, 2009). The danger of oil and gas seepages from abandoned oil wells is a worldwide problem. Approximately 3 million abandoned oil wells are found throughout the United States according to a Stanford study (Johnson, 2015). A recent study conducted at Princeton University claims that many leaking oil wells were found in Northwestern Pennsylvania (Kang et al., 2014). A similar situation occurs in the South Moravian Region of the Czech Republic where oil and gas from improperly sealed abandoned oil leaked to the surface (Smejkalova and Bujok, 2012). In the Gulf of Mexico, there are estimated to be more than 27,000 abandoned oil wells, each having the potential to start leaking oil and gas into the environment (AP, 2010). Part of this research is

to determine how much hydrocarbons are present in the soil next to the wells and if they are currently seeping from the well.

Besides visual detection, several direct and indirect methods are used to detect old oil wells. Different remote sensing techniques can be used to detect changes in soil properties caused by the hydrocarbon contamination over large areas. Remote sensing technology is based on the measurement of reflected or emitted radiation being able to capture fine differences in soil properties due to the different chemical properties in proximity to the leaking oil wells (Jensen, 2006). Petroleum geologists have been increasingly using remote sensing to identify locations where oil and gas are concentrated by identifying the changes in soil and vegetation properties (Yatabe and Fabbri, 1986; van der Meer et al., 2012). The hydrocarbon-induced alterations of the soils and sediments change their spectral signature (reflectance), allowing for identification by the sensors. For geologic remote sensing, much of the focus is on reflected energy within the visual/near infrared (VNIR) wavelengths (0.3-3.0 μm) and on the emitted energy within the far (thermal) infrared (TIR) wavelengths (7.5-13 μm) of the electromagnetic spectrum because this is where most rocks and minerals have characteristic features that can be easily identified (Schumacher, 2000; Jensen, 2006; Nasipuri, 2006; van der Meer et al., 2012).

Physical and chemical changes of the soil with high hydrocarbon content are often caused by mineral precipitation and clay mineral alteration in the soil. These mineralogical changes can be directly detected by X-ray diffraction (XRD) analysis, which is based on the diffraction of X-rays off the crystal structure of a sample (Moore and Reynolds, 1997). The XRD analysis can determine the mineral types present in the soil as well as its percentages (Moore and Reynolds, 1997). Differences in kaolinite and illite content in soil can also be observed in soils with different hydrocarbon content (Schumacher, 1996; van der Meer, 2002; Tangestani and

Validabadi, 2014). There are multiple studies in the literature on the response of spectral signals to the hydrocarbon-contaminated soil.

BACKGROUND

Principles of Remote Sensing

Remote sensing technology is widely used to distinguish chemical and structural properties of Earth's features (Jensen, 2006). Using several different types of sensors, the capability of this technology depends on spatial and spectral resolution of a sensor. Spatial resolution, expressed as an instantaneous field of view, considers a combined spectral signature of all features with in area (i.e. image pixel) (Jensen, 2006). While some commercial satellite sensors have sub-meter spatial resolution (e.g. Quick Bird, GeoEye, Ikonos), many have spatial resolution of 30m (Landsat) or larger (MODIS, SPOT VGT, AVHRR). Coarse spatial resolution masks details on the surface and is often not practical for a given application (Borton, 2007). In addition to spatial resolution, spectral resolution is also important for feature detection. Each sensor is unique for its spectral ranges within which data are acquired (i.e. spectral bands). Multispectral sensors use fewer broad spectral bands while hyperspectral sensors are engineered to collect measurements within very narrow regions or bands (e.g. 10 nm) (van der Meer, 2000).

Band ratios (a.k.a. indices), a ratio created between two or more spectral bands, are commonly used in an empirical approach to detect the properties of Earth's features including water, soil, rocks, and vegetation (Sabins, 1999; van der Meer et al., 2012). This method, where the ratios are correlated with the objects' properties, is widely used to emphasize chemical properties of the ground features while reducing the effect of topography, sensor-target geometry, and shading. In geology, the use of band ratios is considered as a reliable approach in mineral detection (Sabins, 1999; van der Meer et al, 2012). For the detection of hydrocarbon-induced soil alteration, many studies have used band ratios to identify areas with high hydrocarbon contents (Almeida-Filho et al., 2002; Zhang et al., 2009; Zhang et al., 2011; Shi et

al 2012). Although multispectral sensors that acquire data in the near-infrared (e.g. ASTER, WorldView-3) are useful in geology (Shi et al., 2012; van der Meer, 2012; Asadzadeh and Souza Filho, 2016), hyperspectral remote sensing commonly provides more information on soil chemical properties (Duncan and Capps, 2000; Petrovic et al., 2012; Pabón and Souza Filho, 2016). It should be noted that spatial resolution is often a limiting factor despite the high spectral resolution of a hyperspectral sensor. This is particularly important in areas populated by non-active wells or wells with small hydrocarbon seepages.

One of the most widely used satellite sensors is Landsat. The Landsat program started in the early 1970s with the launch of Landsat-1 and continues today with the launch of Landsat-8 in February 2013. Landsat 8 is advantageous due to higher spectral range and radiometric resolution (11 bands; 16 bit) compared to previous Landsat TM satellites (Landsat 7: 8 bands, 8 bit; Landsat 4 and5: 7 bands, 8 bit). Landsat imagery, which has 30m spatial resolution, allows for identification of large scale hydrocarbon seepages, as shown in several studies (Macdonald et al., 1993; Almeida-Filho et al., 2002; Zhang et al., 2009). WorldView-3 is another multispectral sensor launched in 2014. It has a fine spatial resolution of 3.7 m in the infrared region, making it ideal for identifying smaller scale hydrocarbon seeps (Asadzadeh and Filho, 2016). In this study, Landsat data was available and the attempt was made to detect small areas of hydrocarbon contaminated soil using this sensor.

The first hyperspectral sensor was the Scanning Imaging Spectroradiometer (SIS), made in the early 1970s. NASA's Hyperion was launched in 1999 on the Earth Observational (EO)-1 satellite and has been used in several studies concerning hydrocarbon exploration (Duncan and Capps, 2000; Khan and Jacobson, 2008; Smejkalova and Bujok, 2012). HyMap, another hyperspectral instrument developed in the 1990s, has also been used extensively for detecting

hydrocarbon seepages (Horig et al., 2001; Kühn et al., 2004; van der Werff et al., 2007; Petrovic et al., 2012).

In-situ hyperspectral data are commonly used to create hyperspectral libraries of different features in order to advance or validate the satellite-based analyses. For instance, the Spectral Evolutions PSR 3500 spectroradiometer used in this study has a spectral range of 0.4µm-2.5µm using 1023 spectral bands (Spectral Evolutions, 2012a). The fine measurements every several nanometers allows for detection of the soil chemical properties. Several studies used portable hyperspectral instruments to examine the spectral features and effects of hydrocarbons (Chakraborty et al., 2010; Okparanma and Mouazen, 2013; Schwartz et al., 2013; Pabón and Souza Filho, 2016).

Processes of Hydrocarbon Seepages

Pressure differentials and hydrocarbons' lower density drive the hydrocarbons from the reservoir to the surface (Zhenhai et al., 1999; Schumacher, 2000, van der Meer et al., 2000). As they rise through the overlying rock, the hydrocarbons cause alteration of the surrounding rock. The alterations manifest themselves as mineral alterations (such as increase carbonate and clay mineral content, sulfide mineral precipitation, uranium anomalies, bleached red beds), magnetic anomalies, and electrical resistivity anomalies (Schumacher, 1996; Zhenhai et al., 1999; Borton, 2007). The upward migrating hydrocarbons create an alteration column as they travel to the surface, which leaves an alteration halo surrounding the hydrocarbon seepage (Zhenhai et al., 1999).

These hydrocarbon seepages fall into one of two categories: macroseepages and microseepages. While macroseepages are expressed on the surface by oil pools and seepage

along outcrops, microseepages seep vertically or near vertically and leave no physical expression on the surface due to lighter hydrocarbons like methane, ethane, and propane (van der Meer et al, 2002). The wells in Wood County, Ohio exhibit properties from both types of seepages. Wells allow oil and gas to come up directly to the surface where the pools can be observed, while in cases where the wells are cut off below the surface, gases still percolate up through soil and leave no visible surface expression.

In most areas where hydrocarbons come to the surface there are a set of surface expressions that are typically present. Besides high concentrations of methane, ethane/ethene, and propane/propene gasses, hydrocarbon seepages can be directly detected by analyzing mineral alteration in soil and rock, as well as by recording radiometric, temperature, and geobotanical anomalies (Schumacher, 1996; Zhenhai et al., 1999). Monitoring biochemistry of vegetation is on indirect way how hydrocarbon seepages can be detected, which is particularly important in agricultural fields and forested areas where airborne and satellite detection of the wells is obscured by plants (van der Meer et al., 2000). Schumacher (1996) stated that in areas with hydrocarbon microseepages, there can be a wide variety of changes in the soil, including the following: carbonate mineralization, sulfide (particularly pyrite) mineralization, bleaching of red beds, clay mineral alteration, uranium anomalies, magnetic changes, electrochemistry changes, and trace element biochemistry changes. Zhenhai et al. (1999) defined six different surface and near surface expressions of hydrocarbon-induced alteration: hydrocarbon content anomalies in lower atmosphere, hydrocarbon concentration anomalies in the soil, bleached red beds, clay mineral alteration, carbonate anomalies, and thermal inertia anomalies.

Hydrocarbon content anomalies in the lower atmosphere can occur when lighter hydrocarbon gasses accumulate near the surface of the earth. This assumes that conditions are

favorable (low winds and/or an inversion layer) for the hydrocarbon gasses to accumulate. Hydrocarbon anomalies in the soil can also occur, where hydrocarbons can be adsorbed onto mineral grains. This is more stable for those hydrocarbons with longer carbon chains (C_{11} or greater) (Zhenhai et al., 1999).

Bleached red beds occur when hydrocarbons rise through rock, creating a reducing environment where iron oxide minerals like hematite (Fe_2O_3) are reduced to other minerals like pyrite if the hydrocarbons contain sulfur (Zhenhai et al., 1999, van der Meer et al., 2002). Unaltered red beds are characteristically red in color while bleached red beds take on a green-gray color. The reducing environment caused by the high sulfur content can cause pyrite mineralization from iron oxide minerals in the soil. The reaction of hydrogen sulfide with iron oxide ($Fe_3O_4 + H_2S \rightarrow 2FeS_2 + 3H_2O + 2H+ + 2e^-$) causes the iron oxide to reduce and produces pyrite. While pyrite is more common, other sulfide minerals, such as marcasite, sphalerite, galena, pyrrhotite, and native sulfur have also been observed in areas with high sulfur hydrocarbons (Schumacher, 1996).

Due to the acidic reducing environment near the seepage, feldspar minerals can be readily replaced by clay minerals and lead to an increased abundance of clays on the surface. Clay minerals remain stable in certain environmental conditions until those conditions change. The production of CO_2, H_2S, and other organic acids from microbial oxidation of hydrocarbons create reducing environments in the soil, which changes the stability fields (pH and Eh conditions where clay minerals are normally stable) of certain clay minerals (Tangestani and Validabadi, 2014). For instance, normally stable illitic clays commonly changes into kaolinite (Schumacher, 1996; van der Meer, 2002).

The carbonate content anomalies involve bacteria in the soil, breaking down hydrocarbons and release carbon dioxide, which then reacts to form carbonate material. The breakdown of lighter hydrocarbons react with calcium in the area to precipitate calcite in free spaces and pores. Inorganic processes can also lead to carbonate formation. Reactions between hydrocarbons and calcium sulfate ($C_nH_m + 3CaSO_4 \rightarrow {}_3CaCO_3 + CO_2 + H_2O + 2H_2S$) can lead to carbonate formation within the soil and rock (Schumacher, 1996; van der Meer et al., 2000).

Geothermal inertia is the responsiveness of soil to changes in temperature. The emissivity of altered soil is much higher than unaltered soil, increasing the net radiant intensity of local areas (Zhenhai et al., 1999). Oil absorbs energy and then reemits it in the 8-14 μm range of the EM spectrum (Fingas and Brown, 1997). Increased hydrocarbon content changes the thermal conductivity properties, specific heat, and density of the soil, which can cause local anomalies of geothermal inertia (Nasipuri et al., 2006).

Due to the physical and chemical changes, soils with a high hydrocarbon content have a unique reflectance spectral signature (Zhu and Zhang, 1994). There are four distinctive spectral features that are commonly used to determine the presence of hydrocarbons in soils. Two of the spectral features at 1.18 μm and at 1.38 μm, are narrow band spectral regions and less distinctive while the two features at 1.68-1.72 μm and 2.3-2.45 μm are broader spectral regions that are more distinctive and widely used in hydrocarbon characterization (Cloutis, 1989; McCoy et al., 2001; Da-Qi et al., 2008).

Local Geology and Drilling History

The oil and gas wells located in Bowling Green, Ohio are part of the Lima-Indiana oil and gas trend (area where oil and gas wells have been drilled). The source rock (origin) for the

oil and gas in Wood County is the Ordovician age Trenton Limestone formation, which was first named in 1838 by geologist Lardner Vanuxem (Wickstrom et al., 1992). The limestone consists of whole or fragmented fossils in a fine dark-grey to light- brown matrix. The limestone ranges from mudstone to wackestone through packstone to grainstone. Thin black shale beds and styolites are found throughout the formation as well as some secondary dolomitization in some beds (Wickstrom et al., 1992). The Trenton Limestone has variable thickness geographically, ranging from 40 feet in Champaign and Miami Counties to about 300 feet in Ottawa and Lucas Counties. Within Wood County, the limestone ranges from 300 feet in the northern part of the county to 220 feet in the southern most end (Wickstrom et al., 1992). The bedrock for much of Wood County is the Silurian age Lockport Dolomite, which is overlain by a relatively thin bed of glacial till from the last glaciation period (Figure 1) (Norris, 1975). The soil in the study area is made up primarily of the Hoytville clay loam, with a 0-1 degree slope across the entire area (Robbins and Lantz, 2007).

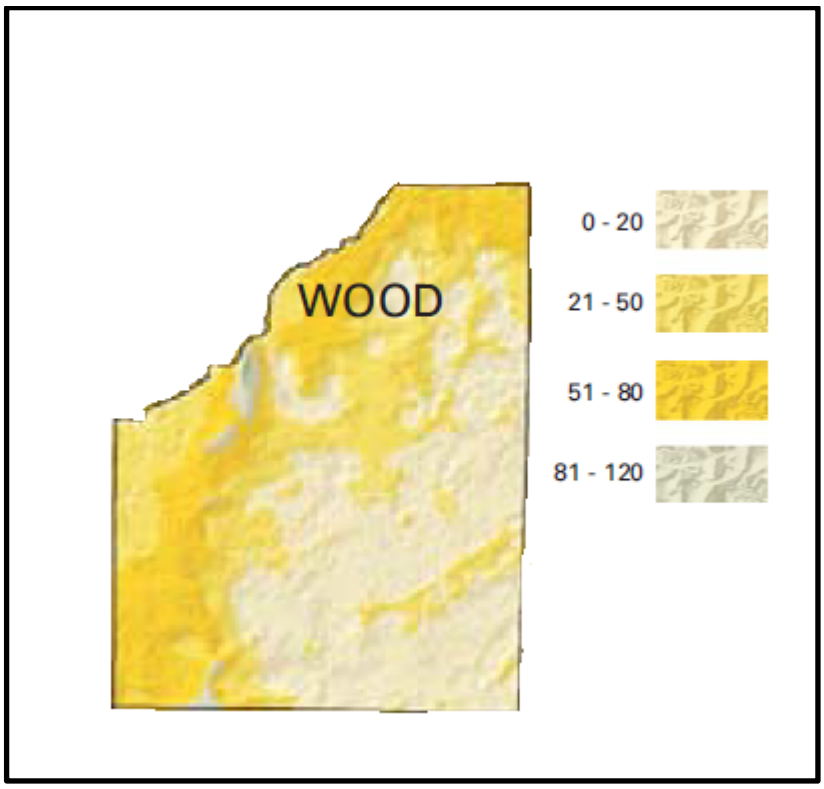

Figure 1: Glacial thickness map of Wood County, Ohio. Depths are given in feet. Modified from ODNR map SG-3, 2004.

The Trenton Limestone lies on the Findlay Arch, which separates the Michigan and Appalachian Basins (Wickstrom et al., 1992). The crest is 15 miles wide in Hancock, Seneca, and Wyandot Counties and broadens northward to 40 miles in Lucas and Ottawa Counties (Wickstrom et al., 1992). The Bowling Green fault is the major structural feature in Wood County and runs underneath the city of Bowling Green. The fault has been variously described as a high angle normal fault, a high angle reverse fault, and a strike-slip fault (Onasch and Kahle, 1991). At one location, the movement was reverse in nature with 250 feet of displacement. At another, there is evidence for left lateral strike slip motion (Norris, 1975). In Wood County, the fault acted as a trap for hydrocarbons by placing the Trenton Limestone against the impermeable shales of the Cincinnati group. With the impermeable Cincinnati Group shales on one side and the Trenton Limestone on the other, this prevented any horizontal movement of hydrocarbons.

Vertical migration was hampered by dolomitization and secondary mineralization at the top of the formation. The fault's porous gouge allowed oil to flow into the traps, creating the reservoirs (Wickstrom et al., 1992).

The Lima-Indiana oil and gas trend extends from Indianapolis in the south along a broad curve to north of Toledo in the north (Figure 2). The oil in the Trenton Limestone has been described as heavy and "sour" (high sulfur content) (Rarick, 1980). There are approximately 60 fields in the Ohio portion of the Lima-Indiana trend, all of which were drilled into the Trenton Limestone (Wickstrom et al., 1992). Commercial quantities of oil and gas in the Lima-Indiana trend were discovered in 1884, just 25 years after the first oil well was drilled in Titusville, Pennsylvania (Wickstrom et al., 1992). Production quickly rose, reaching a peak of 20 million barrels of oil per year in 1896. Cumulative production of the entire trend was estimated to be 500 million barrels of oil, 1 trillion cubic feet of gas, and 1,000,000 wells. There are estimated to be 76,000 wells in the Ohio portion of the trend alone. Two separate booms occurred in the region. The first was the gas boom, which began with the first gas well in 1884 and ended seven years later in 1891. The oil boom started a year after the gas boom began but lasted much longer. The first oil well was drilled into the Trenton Limestone in 1885 and produced 200 barrels of oil at first before settling down to 25 barrels per day, with later wells reaching 5,000-10,000 barrels per day (Wickstrom et al., 1992). The boom ended in 1901 when news of a 100,000 barrel per day gusher discovered near Beaumont, Texas reached the region. When the boom left Ohio, many of the well casings were pulled out, the wells plugged with rocks and stumps, and production moved to Texas (Espen, pers. comm.). The Ohio Oil Company continued to pump oil in the trend until production ceased in 1937 (Wickstrom et al., 1992). The best producing parts of the trend were in Wood and Hancock Counties where recovery of oil reached 14,000 barrels per acre

compared to the average for the Trenton Limestone in Ohio of 1,000 barrels per acre. Problems arose early in the drilling history of then Trenton Limestone because of the oil's high sulfur content. This made it difficult to refine the "sour" crude oil into the more highly desired "sweet" crude oil. This problem was eventually solved in 1899 by J.W. Van Dyke and Herman Frasch, allowing oil production to continue.

Oil drilling and oil storage practices of the time led to significant contamination of the surrounding soil. Drillers followed the "rule of capture", where oil was compared to wild animals in that it was not owned until captured (Wright, 2012). As oil and gas can migrate within the reservoir, wells were drilled in close proximity to each other to pull out as much oil as quickly as possible. After drilling the wells, nitroglycerin was placed in the wells and detonated to release the oil. This would often cause a well blowout, discharging large amounts of oil onto the surface where the oil contaminated the soil and water. The blowout would not be brought under control until the pressure driving the blowout lessened (Rarick, 1980, Wickstrom et al., 1992). In addition to contamination from well blowouts, oil contamination also originated from oil storage tanks, which typically did not have bottoms and were usually made of wood. Leakage and spills from the tanks that contaminated the soil, vegetation, and waterways were common (Rarick, 1980; Wright, 2012). Barges carrying barrels of oil would be floated down streams to processing sites. Dams were built where streams were not deep enough to allow barges to float. These dams were broken on purpose to let the force of the rushing water carry the barges downstream, sometimes causing barges to crash into each other, releasing oil into the environment (Rarick, 1980).

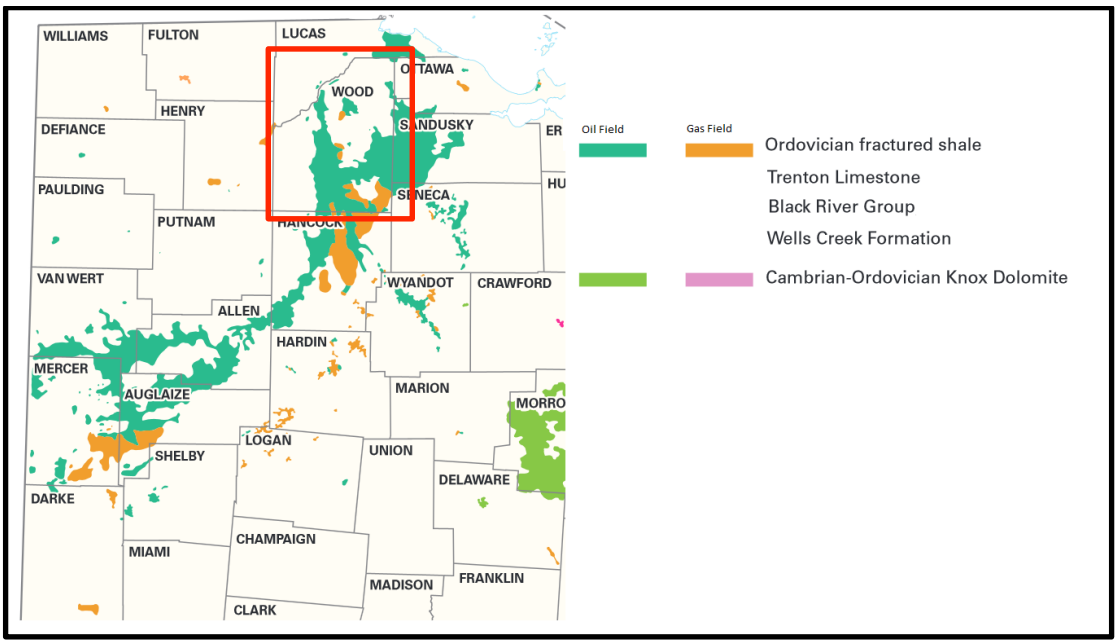

Figure 2: Map of hydrocarbon plays in Northwestern Ohio. The Ohio portion of Lima-Indiana trend extends from Lucas County in the north down in a broad arc to northern Drake County. Wood County is highlighted by red box. Oil and gas from the Trenton Limestone is colored teal and orange respectively. Modified from ODNR Map PG-1, 2004.

Study Objectives

The main objective of this study is to assess the reflectance and chemical properties of soils in proximity of abandoned oil wells located in Northwest Ohio near Bowling Green, Ohio. The goal is to examine the relationship between hyperspectral reflectance measurements and chemical soil properties using X-ray diffraction. It is anticipated that the possible relationship between the reflective and chemical soil properties developed in this study could be used in future studies to enhance the understanding of soil alterations due to hydrocarbon contamination and to enhance the use of remote sensing technology in detection of the wells.

In-situ hyperspectral field measurements are used to examine the spectral regions of interest that are then correlated to soil chemical properties such as hydrocarbon and clay mineral content. In addition, a thermal camera is used to examine surface temperature of the soil with the intention of finding regions with anomalous temperatures indicative of hydrocarbons seeping to

the surface and then correlating them to hydrocarbon contents of the soil. The XRD analysis is designed to identify changes in clay mineralogy and content in clay sized fraction (< 2 μm) of the soils. The effects on soils examined in this study include carbonate mineralization, sulfide mineral precipitation, and clay mineral alteration. The relationship between the lab measured hydrocarbon content and the soil mineralogy is also explored.

This study serves to indicate uncertainties related to limited sampling effort, and to address the importance of field sampling strategies and adequate remote sensing techniques. One of the goals of this research has also been to employ available multispectral satellite data to explore the capabilities of this technology in detecting the abandoned oil wells in Northwest Ohio at large scale. Limited access to commercial data (e.g. WorldView-3) restricted this study to use of Landsat images and in situ hyperspectral data to simulate WorldView-3 datasets both spatially and spectrally.

METHODS

Study Area

Ohio Department of Natural Resources' (ODNR) orphan well list was used to locate wells for this study. A limited number of five wells, located on an agricultural field, in Wood County, Ohio (Figure 3), were available for this study (Figure 4). No coordinates of the study area and oil wells were provided for the reason of privacy protection. The plot is mostly made up of soil belonging to the Hoytville clay loam category (see appendix). The Hoytville clay loam is mostly silt (~42 percent) and clay (~40 percent) with some sand (~15 percent) sized particles (Blevins and Wilding, 1968). The clay sized fraction of the soil is mostly illite (>35 percent) with quartz, vermiculite, kaolinite, and montmorillonite (~5-15 percent each) (Blevins and Wilding, 1968). Iron masses have been reported in the soil (Robbins and Lantz, 2007), which when subjected to a reducing environment caused by hydrocarbons can alter into pyrite and other iron sulfide minerals.

Wells 1 and 2 were located close to the road while wells 3, 4, and 5 are located farther north in the plot. Well 1's casing was cut off at the surface and bent shut, while the casings for wells 2, 3, and 4 extended above ground. Well 5 was flush with the ground, having no visible casing above the ground. The well was open and the surrounding soil and vegetation was coated in black residue, presumably from the well. A strong rotten egg/asphalt odor was noticed coming from all the wells.

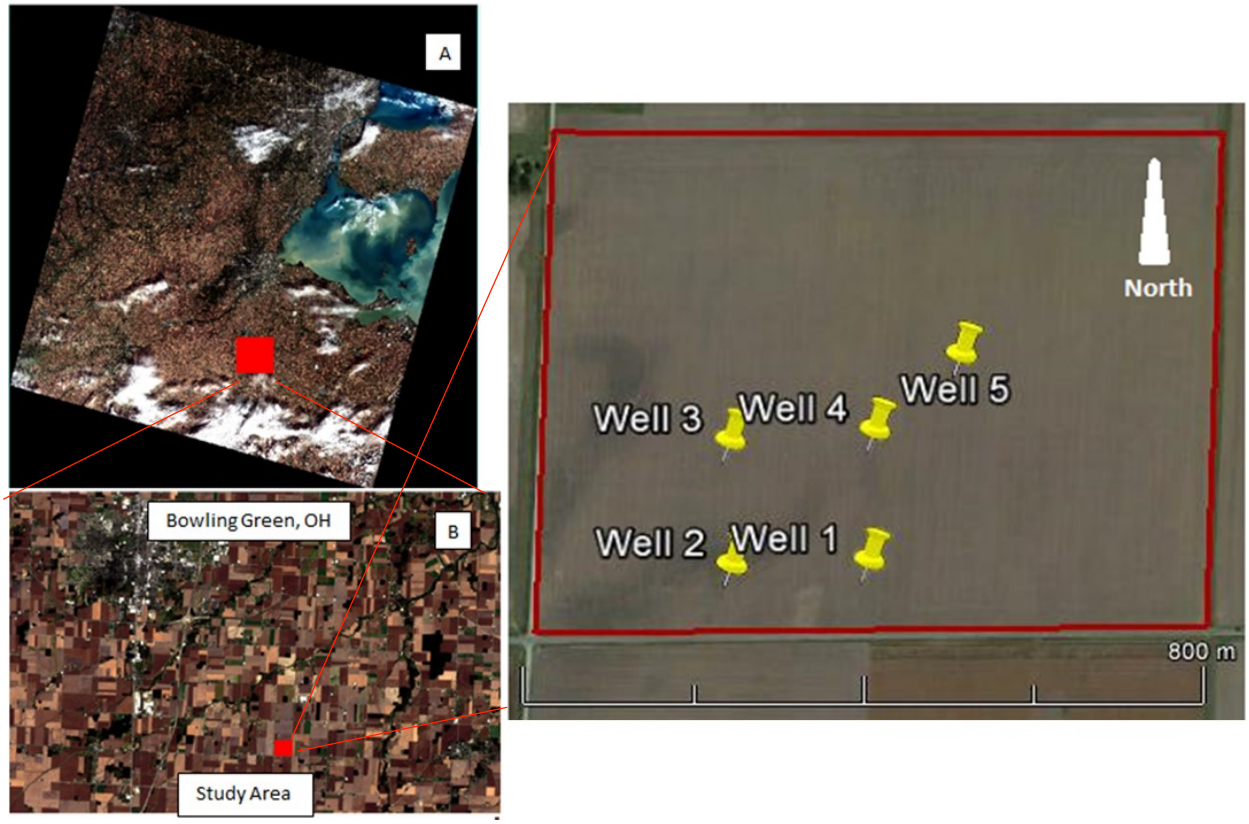

Figure 3: Location of study area near Bowling Green, OH. (A and B) Landsat-8 image dated October 8, 2015 (image width is 185 km). (C) The study site (Source: Google Earth). Note that the number of wells were limited in this study.

Figure 4: Photograph of wells: well 1 (A), well 2 (B), well 3 (C), well 4 (D), well 5 (E). Note the darker soil and black residue around well 5

To assess the reflectance and chemical properties of the soil, the following methods were employed: satellite remote sensing using Landsat-8, in situ hyperspectral remote sensing using a portable spectroradiometer, thermal imaging using a single band camera, and X-ray diffraction (XRD) analysis to examine the clay sized fraction of the soils surrounding the wells. Hydrocarbon content analysis was performed to determine the levels and types of hydrocarbons in the soil to compare against the other methods. In addition, it was expected that this analysis

could detect if the soil contamination is due to recent oil seepage from the well or due to the residues from oil drilling processes that might have occurred in the past.

EPA 8015 Diesel Range Organics/Oil Range Organics (DRO/ORO)

Soil samples were collected for hydrocarbon content analysis from each well. Due to limited funding, the number of soil samples were restricted to one sample per well. Soil was taken at several locations focusing on the area within 1 m from the well where hydrocarbons were expected to be concentrated. Four to five samples were homogenized to create a representative sample for each well. Samples were taken at three different dates for wells 1-4 (5/3/15, 8/4/15, and 10/8/15). Well 5 was not originally on the list and was added to the collection in the later phases (10/8/15). Data collection on 5/3 was different from the other two collection dates in that soil was collected out to 3 m from the well instead of within 1 m like the other dates. A control sample was created by taking soil from several presumably uncontaminated locations in the field (at least 30 m from any well) to create a representative sample for the field. Immediately after collection, the samples were packed on ice into tightly sealed glass jars to prevent hydrocarbon volatilization and sent to Advanced Analytics Laboratories in Columbus, Ohio. EPA 8015 Diesel Range Organics (DRO) and EPA 8015 Oil Range Organics (ORO) methods were used to determine the amount of hydrocarbons in the samples. Results were given in mg/kg with a reporting limit of 11.6 mg/kg. The DRO test analyzes for C10-C20 hydrocarbons while the ORO test analyzes for C20-C34 hydrocarbons. For the purpose of this study, only samples collected on October 8, 2015 were used for analysis in conjunction with XRD, thermal, and spectral reflectance analysis. To determine statistical significance of the hydrocarbon content values, samples from all collection dates were used.

In Situ Hyperspectral Field Data Collection

A Spectral Evolution spectroradiometer PSR 3500 was used for in situ measurements of the soil reflectance. The instrument has a spectral range of 0.35 μm to 2.5 μm and collects the spectral data with a resolution of 1.5 nm for the spectral range of .35-1.000 μm, 3.8 nm at 1.500 μm, and 2.5 nm at 2.100 μm (Spectral Evolution, 2012a). Soil reflectance measurements were taken in four directions (north, south, east, and west) from the well at $\leq$ 1 m, 3 m, 5 m, 10 m, 20 m, and > 30 m increments (Figure 5). The instrument was set to take average 10 readings per measurement. Two spectral reflectance measurements were taken at each measurement location and averaged for each location. The spectral reflectance data were analyzed using Spectral Evolutions, Inc. DARWin v. 1.2 software (Spectral Evolution, 2012b). The spectral signatures were examined to identify the spectral behavior of the soil.

A band ratio (index) was created from each spectral signature using average reflectance of two bands, one covering the spectral range from 2.211 μm 2.223 μm and another including the spectral region between 2.309 μm and 2.346 μm. This index will be hereafter referred to as the "*hyperspectral index"*. The bands were chosen based on the visual analysis of the spectral signatures and detection of the region where signals between the control and near-well sample locations differed. A slope analysis between two designated bands were conducted and the results between the control and near-well sample locations compared. Visual examination of the slope between the two spectral bands indicates a linear slope. The analysis was based on the slopes of the average reflectance for 2.211 μm-2.223 μm and 2.309 μm-2.346 μm.

To simulate the WorldView-3 spectral signatures, the hyperspectral reflectance data were spectrally aggregated to model the short-wave infrared (SWIR) bands 6 (2.185-2.225 μm) and 8

(2.295-2.365 µm) of the WorldView-3 satellite. SWIR bands 6 and 8 of WorldView-3 were chosen based on the designated spectral regions of hyperspectral signatures as previously reported (see Figure 6). These two bands were used to create an index of SWIR 6 / SWIR 8, hereafter referred to as *"multispectral index"*. The spatial resolution of the SWIR bands is 3.7 m, which was simulated by combining the spectral reflectance measurements of 1 m and 3 m for each direction from the well. The modeled bands are related to other field and lab measurements.

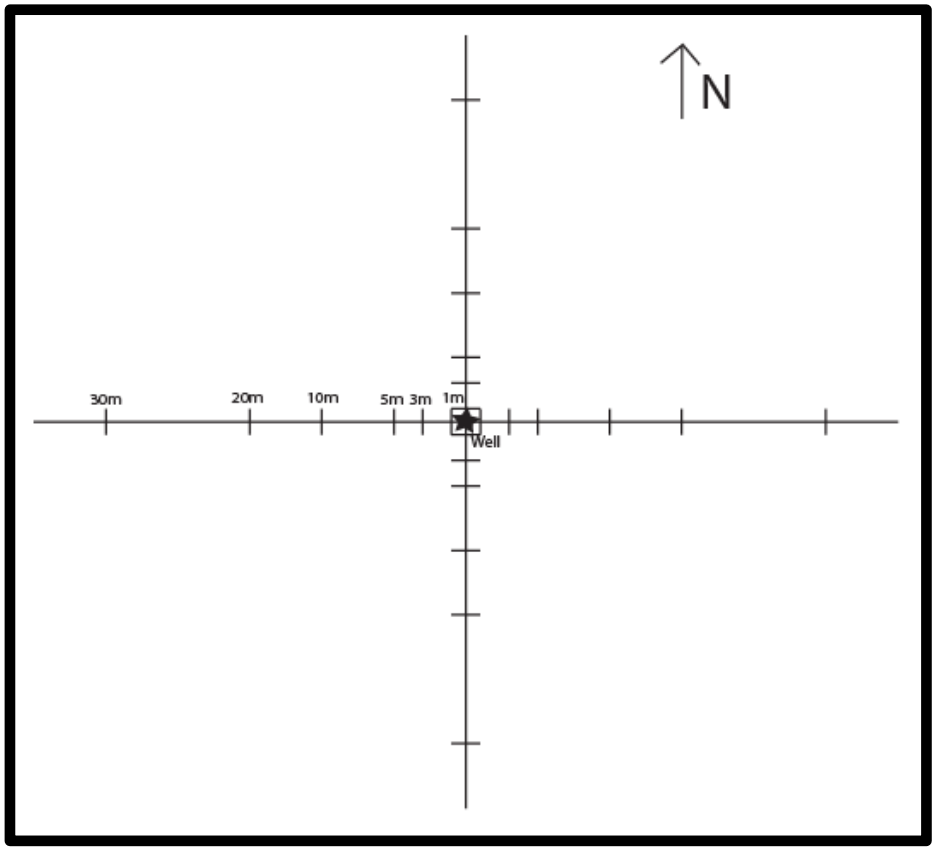

Figure 5: Diagram showing data collection scheme for hyperspectral measurement. Star at center represents the well. Soil samples were taken within 1 m of the well while a control sample was taken > 30 m from the wells. Thermal readings were taken at the well and at 5 m from the well.

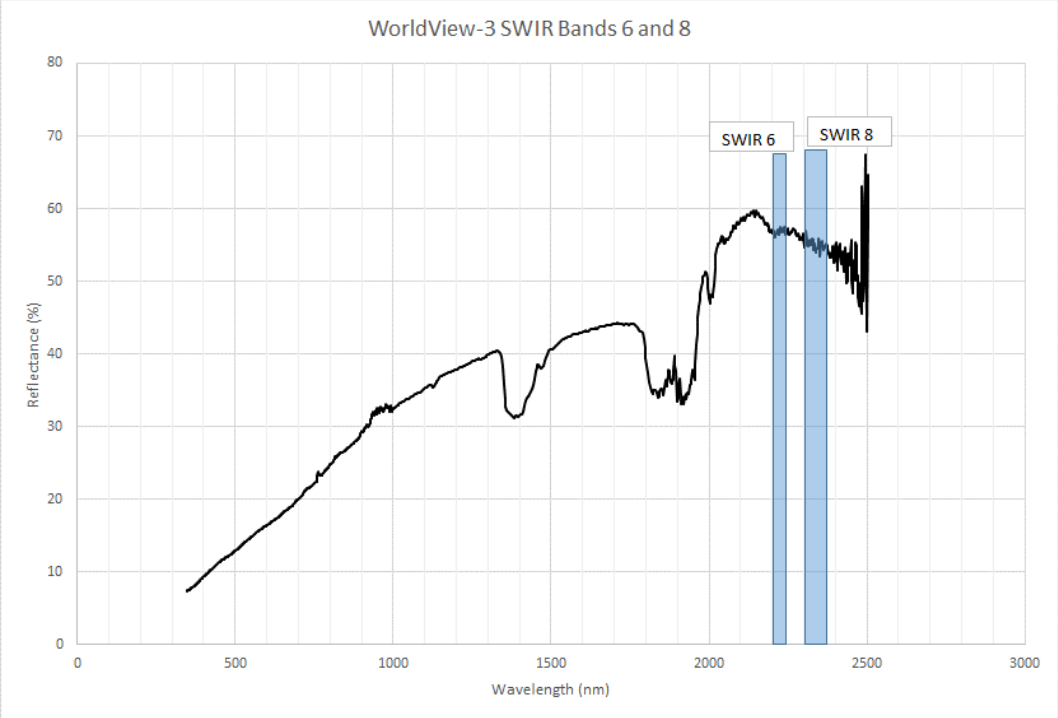

Figure 6: Spectral signature of soil with WorldView-3 bands superimposed over their respective band widths.

X-ray Diffraction

X-ray diffraction analysis was used to analyze the clay sized fraction of the soils sampled from around the wells. Clay sized particles (< 2 μm) were separated from the rest of the soil sample by gravitational settling method. Soil from the study area was mixed with 20.0 ml of dispersant (sodium metahexaphosphate) and 250 ml of distilled water. After mixing and letting stand for 10 minutes, the slurry was transferred to a 1-liter graduated cylinder and distilled water added to bring up to the 1 liter mark, where the entire slurry was thoroughly mixed. The top 10 cm of the water column was drawn off after eight hours and put aside, after which the cylinder refilled and the process repeated. The top 10 cm were removed both times because clay minerals can only settle about 10 cm in 8 hours. The clay-rich solution from both settling trials was transferred to a beaker, to which a concentrated NaCl solution was added to flocculate the clay

particles. After the clays fell out of suspension, the supernatant liquid was drawn off and discarded.

The glass side method was used for the XRD samples. Three samples were created for each soil sample. One sample was treated with 1N MgCl solution, precipitated onto a glass slide, and left to air dry at room temperature. Treatment with Mg is standard for XRD analysis because different clay minerals react differently to Mg within the layers of the clay. Another sample was also treated with 1N MgCl solution, precipitated onto a glass slide and left to air-dry. Afterwards, it was treated in an ethylene glycol chamber for 8 hours. The treatment with ethylene glycol was done to see if there were any swelling clays (smectite and montmorillonite) in the sample, which on analysis, would increase the spacing between the clay layers. The last sample was treated with a 1N KCl solution, precipitated onto a ceramic streak plate, and baked in an oven at 550 ^{0}C for two hours. This process was done because it would collapse any expandable layers within the clays and destroy the peaks of certain minerals (like kaolinite), allowing for identification later (Moore and Reynolds, 1997). The samples on the streak plate were transferred to a glass slide and glued using Duco cement because the mount inside the XRD unit could not focus correctly on the sample when it was on the streak plate. Samples were then run through the X-ray diffractometer, scanning from 4.000-35.000 degrees 2θ at a scan speed of 1.500 2θ/min, measuring every 0.02 degrees 2θ. This 2θ range was chosen because most of the diagnostic peaks for clay minerals are present this region. Any quartz found in the samples will compared to a quartz standard to determine analytical uncertainties.

After the samples were analyzed in the X-ray diffractometer, the data were transferred to Rigaku's PDXL integrated X-ray powder diffraction software (Rigaku, 2011). Diffractograms from each sample were analyzed for clay mineralogy and a quantitative analysis was done using

the reference intensity ratio (RIR) method. Individual minerals were chosen based on their intensity counts, peak position, and figure of merit (FOM) values. Figure of merit, in this case, is a calculated value that characterizes the closeness of a match between a candidate mineral and the sample being measured. The PDXL software generates possible candidates that possibly match the sample and each is given a FOM value. Factors taken into account when calculating FOM for each possible candidate include the number of peaks that match between the candidate and the sample, how well the candidate's and sample's peak intensities match, and a calculation of the number of peaks present versus number possible in the analysis area. Lower FOM values indicate a better match between the candidate and the sample (Fawcett et al., 2011).

Thermal Imaging

Thermal images were taken at each well using a FLIR E40bx single band thermal camera to measure surface temperature at the sampling points. Images were taken on October 8, 2015 at specific distances (0 m and 5 m) from the well at a height of 0.5 m in order to create an image that covers about 1 m. Images were taken at dusk on a dry day, several days after the most recent precipitation to avoid water influence on the emissivity of the soils (van der Meijde et al, 2013). The camera measures emissivity of the soil with a single spectral band of 7.5 μm-13 μm with a thermal sensitivity of <0.045 ^{0}C at 30 ^{0}C. The thermal images were analyzed using FLIR Tools Software to analyze the surface temperature at each well (FLIR, 2016).

Satellite Remote Sensing Using Landsat-8

A Landsat-8 image of the study area dated October 8, 2015 was downloaded from the United States Geological Survey's GloVis satellite imagery database. The satellite image was

chosen after the crops (soybeans) was harvested, reducing the influence of vegetation on the signal. Radiometric and atmospheric corrections were performed using ENVI 5.2 software and its Fast Line-of-sight Atmospheric Analysis of Spectral Hypercubes (FLAASH) module. Three mineral indices (band ratios) were calculated [clay mineral (band 7 / band 6), ferrous iron minerals (band 5 / band 4), and iron oxide (band 4 / band 2)] in an attempt to identify possible spectral anomalies related to hydrocarbon-induced soil alteration in the Landsat-8 image. The mineral indices were designed to highlight certain mineralogical features in the image, and were used in an empirical approach. In this approach indices related to properties of the feature can suggest areas where soils have been altered by hydrocarbons.

Statistical Analysis

Statistical analysis was done on all data to determine significance and correlation of the methods used. T-test analyses, assuming unequal variances, at the 95 percent confidence level were run on all data sets to determine statistical significance between the mean values of the measurement at different sample locations. The correlation analyses were performed to examine correlation between reflectance parameters and soil chemistry. The Pearson correlation coefficient (r) and coefficient of determination (r^2) values were calculated to examine the correlation between soil spectral properties and chemical properties as well as possible predictively of soil chemistry using spectral bands. The number of samples used in this study was below the optimal number needed to derive solid conclusions. Additional data collection was not possible due to several reasons. Correlation coefficient (r) values were also calculated for the clay mineral content and thermal values. Coefficient of determination (r^2) was used to

examine the regression between the soil hydrocarbon content and both hyperspectral and multispectral indices.

RESULTS

Soil Hydrocarbon Content Analysis

The results of the soil hydrocarbon content lab analysis are summarized in Table 1. Results shown are from the EPA 8015 ORO test. The DRO range hydrocarbons were below detection limits (10.7 mg/kg). The soil hydrocarbon content from the May collection date is lower than data collection from August and October due to different distances of the data collection from the well (within 3 m). The total hydrocarbon content for the control samples ranged from 30.1-37.7 mg/kg (average: 33.9 mg/kg). The soil hydrocarbon content for August and October ranges between 660 mg/kg for well 1 and 5680 mg/kg for well 4 with the average being 2768 mg/kg for all wells. Hydrocarbon content is higher in the August samples date than the samples taken in October. Several trends in the data are evident. One trend shows that samples from well 1 generally have a lower hydrocarbon content the other wells. Another data trend indicates that well 2 generally has a higher hydrocarbon content than the other wells (except the August sample, where well 4 is higher). The hydrocarbon content differences between the wells and the control soil sample are statistically significant when all wells are considered, given that only one sample was collected and analyzed for each site (Table 2). With the exception of the well 1 content of the October collection, all of the wells have a similar hydrocarbon concentration.

Table 1: Hydrocarbon concentrations for each well on collection date. Note: For statistical analysis, only samples collected on 10/8/15 are used when comparing to clay minerals. All values are used for determining overall statistical significance. *Note: Sample collection in May was performed within 3 m distance from the wells compared to within 1 m for other dates.

Well 1 hydrocarbon concentrations			
At well		control	
date	concentration (mg/kg)	date	concentration (mg/kg)
10/8/2015	660	9/27/2015	37.7
8/4/2015	1210	5/3/2015	30.1
5/3/2015*	363	Average	33.9
Well 2 hydrocarbon concentrations			
At well		control	
date	concentration (mg/kg)	date	concentration (mg/kg)
10/8/2015	2570	9/27/2015	37.7
8/4/2015	4750	5/3/2015	30.1
5/3/2015*	545	Average	33.9
Well 3 hydrocarbon concentrations			
At well		control	
date	concentration (mg/kg)	date	concentration (mg/kg)
10/8/2015	2260	9/27/2015	37.7
8/4/2015	3520	5/3/2015	30.1
5/3/2015*	386	Average	33.9
Well 4 hydrocarbon concentrations			
At well		control	
date	concentration (mg/kg)	date	concentration (mg/kg)
10/8/2015	2130	9/27/2015	37.7
8/4/2015	5680	5/3/2015	30.1
5/3/2015*	200	Average	33.9
Well 5 hydrocarbon concentrations			
At well		control	
date	concentration (mg/kg)	date	concentration (mg/kg)
10/8/2015	2170	9/27/2015	37.7

Table 2: P-values from t-test used to compare the measurements between wells and control soil sample at 0.95 confidence level. Note that significance test for hydrocarbon content, kaolinite content, and illite content are for all wells, not individually. Asterisk (*) shows non-significant relationships.

	Wells					
Measurements	1	2	3	4	5	all wells
Hydrocarbon content	NA	NA	NA	NA	NA	0.0024
Hyperspectral Slope	0.0045	0.0900*	0.0104	3.321E-04	0.0094	1.48E-07
Hyperspectral Index	0.0016	0.248*	0.0363	4.573E-04	0.0030	4.28E-07
WorldView-3 Index	0.037	0.2847*	0.0165	9.506E-04	0.0122	3.43E-04
Temperature	5.6E-10	7.65E-09	0.0039	NA	1.288E-04	5.47E-07
XRD: Kaolinite	NA	NA	NA	NA	NA	0.0013
XRD: Illite	NA	NA	NA	NA	NA	0.0018

Hyperspectral Field Spectra Analysis

After visual observation of the signatures, spectral features at 1.4 µm, 1.8 µm, and 2.2-2.3 µm are analyzed. Figures 7-11 show the spectral signatures acquired for different measurement distances from the wells. There are variations in the spectral signature around 2.3 µm region in measurements taken close to the wells, generally within 3 m of the wells. Using the average reflectance of the two spectral bands of the hyperspectral index in the slope analysis (see Methods), the slope change in the spectral signature around 2.3 µm was examined. The slope analysis reveals that at there is a statistically significant difference between the slopes at 1 m and > 30 m for all wells individually except well 2.

The band ratio values for the hyperspectral index can be found in Table 5-9. In addition to the slope analysis, a statistically significant difference was found for the index values between 1 m and > 30 m as well. The same significant trend is observed for both methods suggesting

there is a difference between the soils near the well and soil far from the well. The band ratio values show significant differences for all wells, including well 2.

There are a number of trends in the data. Slope values between the spectral bands tended to be steeper (overall average slope: -3.277) for measurements taken 1 m from the wells while slope values for the >30 m measurements were generally lower (overall average slope: -0.842). The slope values of soil reflectance within 1 m are highest at wells 1 and 5 (-4.278 and -4.938 respectively) (Table 4 and Table 12 respectively). Soil with a higher hydrocarbon contents do not necessarily indicate a higher slope value. Well 1 has the lowest hydrocarbon content of the wells (October; Table 1) but has a higher average slope value than the most of the other wells (Table 4). Well 3, having the highest hydrocarbon content, has among the lowest slope values for soil within 1 m of all the wells (average: -2.403) (Table 8). Of the slope values for soil measurements taken beyond 30 m from the wells, well 5 has the highest slope values (average: -1.822) (Table 12).

Hyperspectral band ratio values, based on the ratio of 2.211-2.223 μm / 2.309-2.326 μm, tend to be higher (average values: 1.06) in measurements taken within 1 m from the wells. For beyond 30 m, the index values are lower with the average at 1.02. Wells 1, 4, and 5 produce the highest index values of the wells (averages: 1.076, 1.07, and 1.079 respectively) (Tables 5, 11, and 13 respectively). The soil around well 3 (October) has a higher hydrocarbon content then wells 1, 4, and 5 (Table 1) yet did not have the highest index values (average: 1.047; Table 9). Well 5 has the highest average index values (Table 13). Well 1 has the lowest hydrocarbon content (Table 1) yet index values from soil within 1 m of the well were relatively high (Table 5). Well 2 is different from the other wells. Index values calculated from soil reflectance greater than 30 m from the well are, on average, higher (average >30 m: 1.048) than index values

calculated from the 1 m measurements (average: 1.039) (Table 7). The band ratio value based on the measurement taken in the west direction is considerably high compared to the other directions. The possible reasons for this trend are discussed later.

A weak coefficient of determination value was found between the hydrocarbon content and the slope values (r^2=0.356) (Table 3). The correlation coefficient for the same parameters generates a reasonable correlation (slope values: r = -0.596). A relatively strong correlation was found between the hydrocarbon content and the hyperspectral index values (r^2=0.743). Although statistically similar variables, slope and hyperspectral index exhibit different prediction capabilities.

It is important to emphasize once again that the statistical results for well 2 behave differently than for the other wells in several aspects. For well 2, only the temperature values between thermal images taken at the well and thermal images taken 5 m away were significant; all other values show non-significant relationships between soil hydrocarbon content versus slope analysis, soil hydrocarbon versus and multispectral index, and soil hydrocarbon content versus hyperspectral index (Table 2). Removing well 2's data from the analysis related to both hyperspectral and multispectral indices, the r^2 values increase (Tables 3 and 26).

Table 3: Coefficient of determination values (r^2) examining the predicative relationship between soil hydrocarbon content and slope values and between soil hydrocarbon content and hyperspectral index.

Coefficient of determination (r^2 values)	Hydrocarbon Content (without well 2 included)	Hydrocarbon Content (with well 2 included)
Slope Values	0.356	0.356
Hyperspectral Index	0.743	0.473

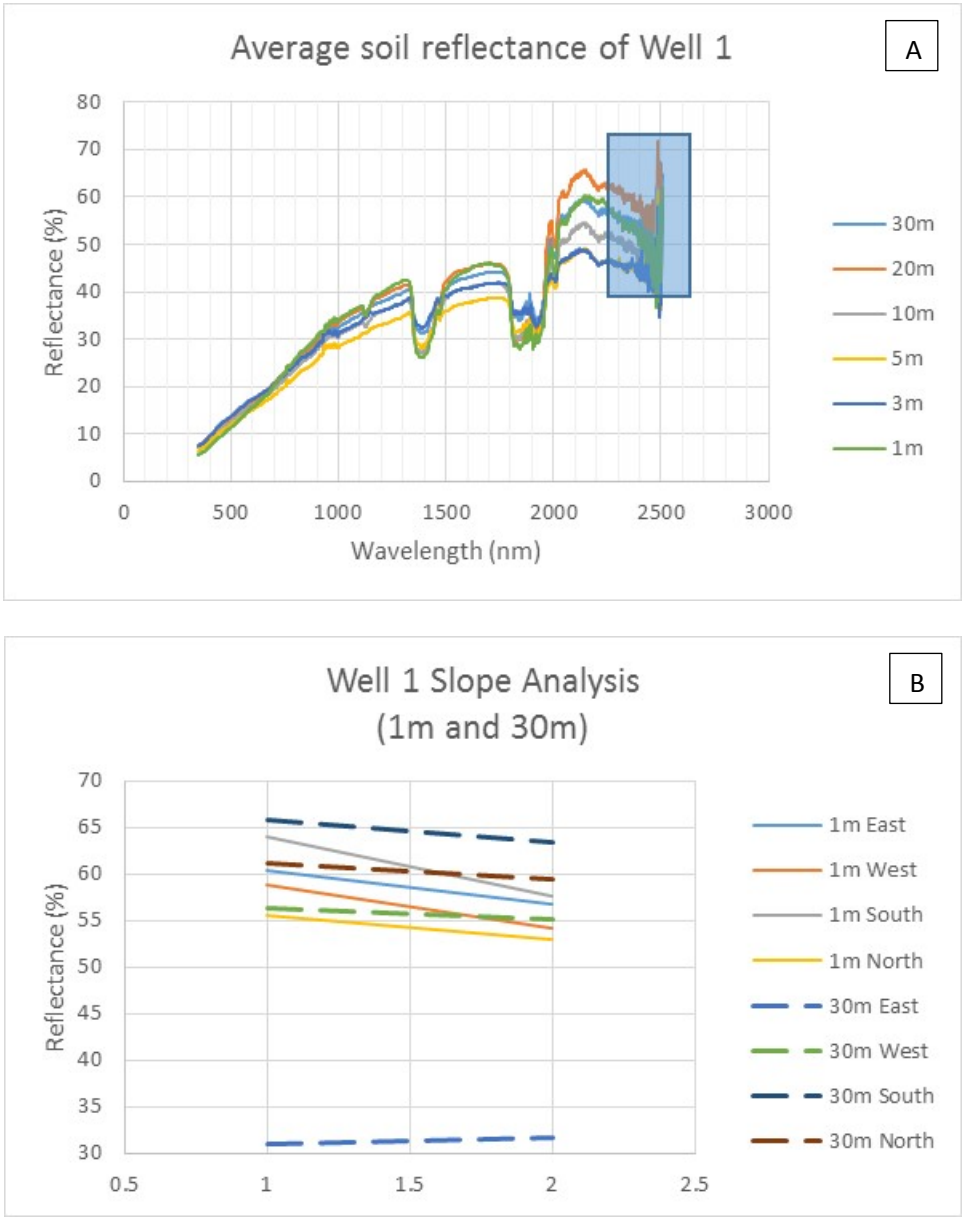

Figure 7: Soil spectral reflectance of well 1 at various distances. (A) Well 1 average soil reflectance for each measurement distance from the well, (B) Slopes between the spectral bands.

Table 4: Slope values for lines shown in Figure 7b.

Slope values	East	West	South	North	Average	Standard Deviation
1 m Average	-3.55	-4.651	-6.308	-2.603	-4.278	2.174
>30 m Average	0.689	-1.21	-2.374	-1.831	-1.247	1.641

Table 5: Well 1 hyperspectral index values (2.211-2.223 µm /2.309-2.326 µm).

Hyperspectral Index	East	West	South	North	Average	Standard Deviation
1 m	1.096	1.100	1.135	1.047	1.076	0.034
	1.033	1.066	1.081	1.051		
> 30m	0.978	1.011	1.053	1.040	1.022	0.024
		1.036	1.018	1.018		

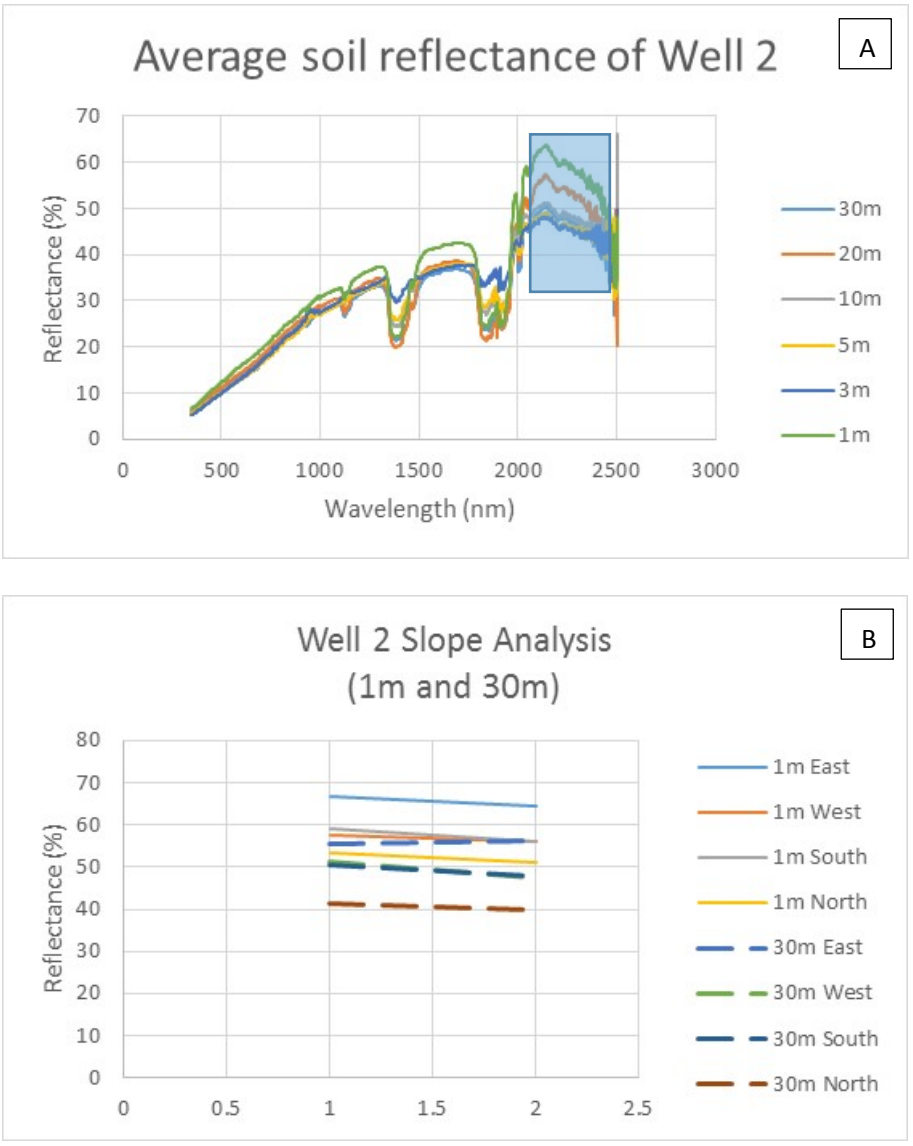

Figure 8: Soil spectral reflectance of well 2 at various distances. (A) Well 2 average soil reflectance for each measurement distance from well, (B) Slopes between the spectral bands.

Table 6: Slope values for lines shown in Figure 8b.

Slope Values	East	West	South	North	Average	Standard Deviation
1 m Average	-2.454	-1.478	-3.017	-2.022	-4.278	0.739
> 30m Average	0.691	-3.581	-2.623	-1.676	-1.798	1.736

Table 7: Well 2 hyperspectral index values (2.211-2.223 μm /2.309-2.326 μm).

Hyperspectral Index	East	West	South	North	Average	Standard Deviation
1 m	1.034	1.027	1.043	1.034	1.039	0.012
	1.044	1.025	1.063	1.046		
> 30m	0.978	1.078	1.049	1.046	1.048	0.032
	1.058	1.078	1.061	1.037		

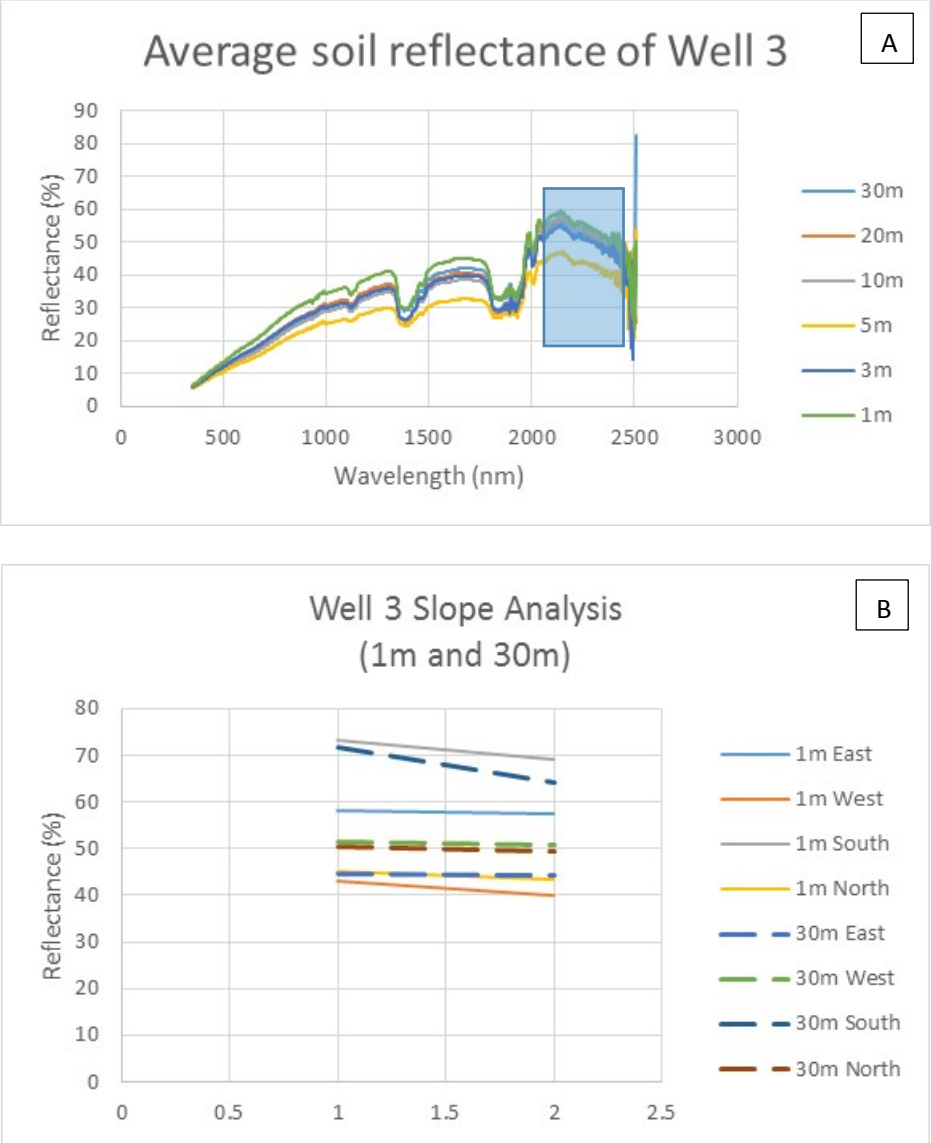

Figure 9: Soil spectral reflectance of well 3 at various distances. (A) Well 3 average soil reflectance for each measurement distance from well, (B) Slopes between the spectral bands.

Table 8: Slope values for lines shown in Figure 9b.

Slope Values	East	West	South	North	Average	Standard Deviation
1 m Average	-0.793	-2.988	-4.066	-1.764	-2.403	1.379
> 30m Average	-0.115	-0.649	-7.627	-1.210	-0.658	1.073

Table 9: Well 3 hyperspectral Index values (2.211-2.223 µm /2.309-2.326 µm).

Hyperspectral Index	East	West	South	North	Average	Standard Deviation
1 m	1.014	1.067	1.063	1.034	1.047	0.027
	1.014	1.081	1.054	1.052		
> 30m	1.023	1.020		1.046	1.022	0.023
	0.987	1.007		1.048		

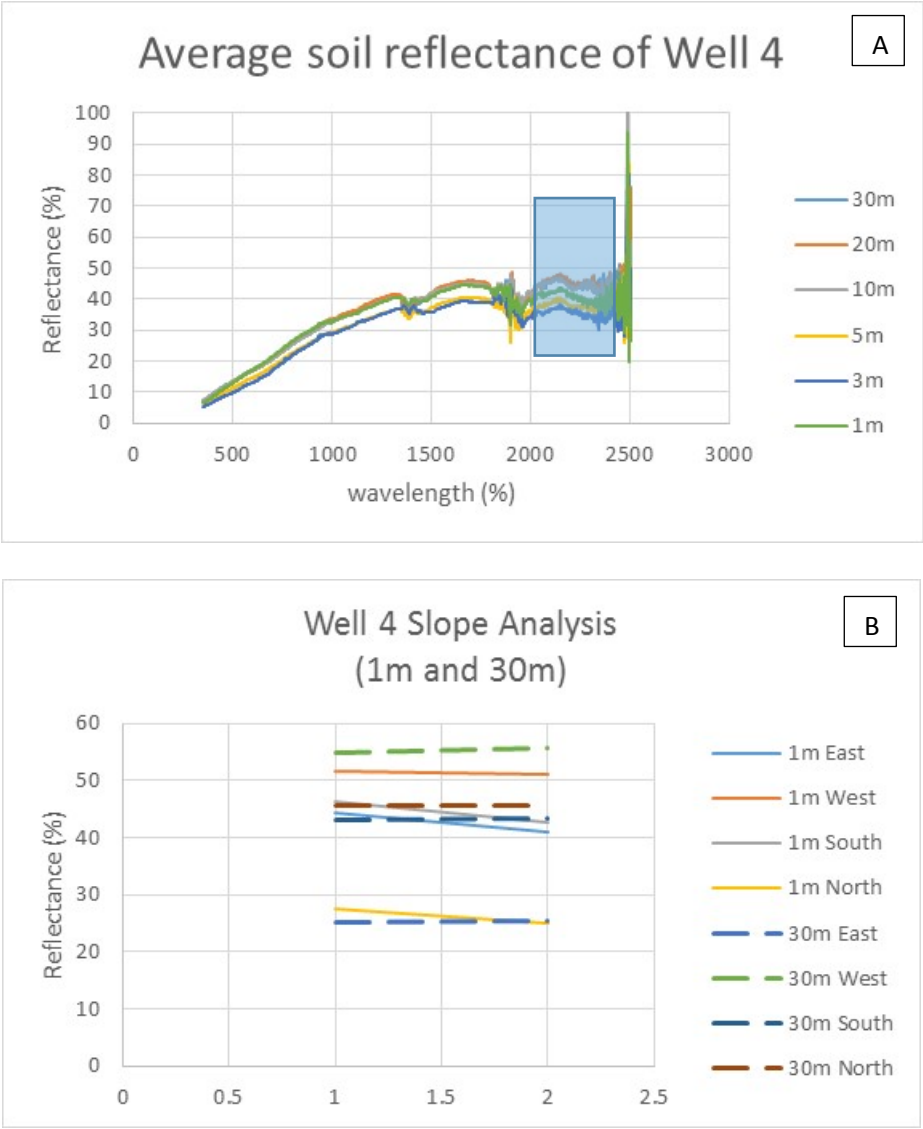

Figure 10: Soil spectral reflectance of well 4 at various distances. (A) Well 4 average soil reflectance for each measurement distance from well, (B) Slopes between the spectral bands.

Table 10: Slope values for lines shown in Figure 10b.

Slope Values	East	West	South	North	Average	Standard Deviation
1 m Average	-3.552	-0.649	-3.491	-2.405	-2.524	1.675
> 30m Average	0.225	0.757	0.105	0.593	0.626	1.012

Table 11: Well 4 hyperspectral index values (2.211-2.223 µm /2.309-2.326 µm).

Hyperspectral Index	East	West	South	North	Average	Standard Deviation
1 m	1.064	1.023	1.116	1.092	1.07	0.041
	1.103	1.004	1.052	1.104		
> 30m	0.991	1.015	1.032	1.011	0.994	0.024
	0.991	0.959	0.972	0.984		

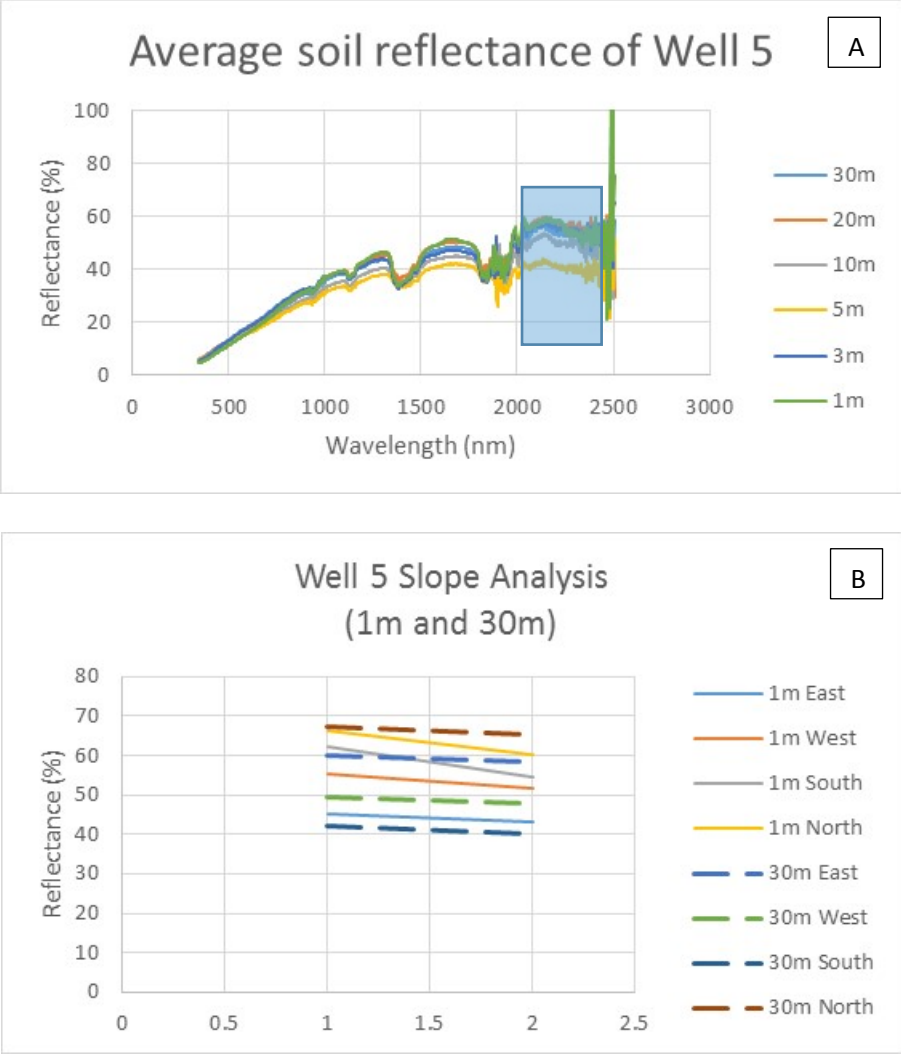

Figure 11: Soil spectral reflectance of well 3 at various distances. (A) Well 5 average soil reflectance for each measurement distance from well, (B) Slopes between the spectral bands.

Table 12: Slope values for lines shown in Figure 11b.

Slope Values	East	West	South	North	Average	Standard Deviation
1 m Average	-1.933	-3.770	-7.717	-6.331	-4.978	2.741
> 30m Average	-1.572	-1.872	-2.081	-1.764	-1.822	1.734

Table 13: Well 5 hyperspectral Index values (2.211-2.223 μm /2.309-2.326 μm).

Hyperspectral Index	East	West	South	North	Average	Standard Deviation
1 m	1.055	1.026	1.166	1.115	1.094	0.026
	1.036	1.134	1.121	1.099		
> 30m	0.979	1.040	1.090	1.019	1.022	0.023
	0.974	1.025	1.016	1.036		

To further explore the cause of the changes in the slope observed within the near-infrared region, the reflectance of the clay sized fraction soil samples were measured. The identical spectral region and same ratios (index) as previously used were compared with the in situ hyperspectral reflectance soil measurements taken in the field. Results of the index show that there is no statistical difference in reflectance measurements between the clay sized fraction control soil samples and the clay sized fraction near-well samples (Table 14). There is also no statistical difference in reflectance measurements between the clay sized fraction control sample and the in situ measurements at > 30 m distance from the wells (Table 14). The results did show that there is a statistical difference in reflectance measurements between the clay sized fraction samples taken from soil directly next to the well and the in situ 1 m reflectance measurement.

Table 14: T-test analysis: In-situ soil reflectance and clay sized fraction soil reflectance at 0.95 confidence level.

t-Test for different sample combinations	P value
> 30m (in situ)-Control (clay sized)	0.1437
Control (clay sized) - Wells (clay sized)	0.1472
Wells (clay sized) - Wells (in situ)	0.0092

Mineral X-ray Diffraction Analysis

The diffractograms from the XRD analysis can be found in Figures 12 – 17. Four minerals were identified, namely quartz, kaolinite, illite, and vermiculite. There is no difference in the clay mineralogy between wells and the control. Table 15 shows the FOM for each mineral in the analysis. The peaks at 6 degrees 2θ was determined to be associated with vermiculite, which had a d-spacing of 14 angstroms. There was no changes in the d-spacing when the samples were treated with ethylene glycol, indicating that the peaks belong to vermiculite and not a swelling clay mineral like montmorillonite. The peaks at 9, 18, and 26 degrees 2θ are illite peaks. The kaolinite peaks are located at 12 and 24 degrees 2θ. The peaks for quartz are at 21 and 26 degrees 2θ. Calcite and or dolomite should have been present in the soil samples as well because the bed rock is the Lockport dolomite, which is only a few meters below the surface. These mineral phases are not identified because their peaks are not present in the XRD analysis, most likely because only the clay sized fraction of the soil is analyzed. Wells 2 and 5 had an anomalous peak at 32 degrees 2θ. No clay mineral or other minerals that might possible be in the soil can account for the peak in that region. It is possible that the peak corresponds to some contaminate from sample collection or from sample preparation.

The quantitative analysis using the RIR method found that in the clean (control) samples, there is a higher content of kaolinite (36%) compared to the samples taken from near the wells (between 14% and 28%). Table 16 provides mineral content for each sample. However, the illite content of the soil is higher at the wells (53%-70%) than in the control sample (45%). Quartz and vermiculite remain generally unchanged across the samples (11-19% and 0.7-1.7% respectively).

The illite and kaolinite contents are statistically significant (Table 2). Kaolinite and illite contents correlate well with the hydrocarbon contents ($r = -0.873$, $r = 0.846$ respectively), with

kaolinite having a strong negative correlation and illite having a strong positive correlation (Table 17). This indicate that the kaolinite and illite contents within the clay sized fraction are changing depending on the presence on hydrocarbons in the soil. Well 2 is different from the rest because it has a relatively higher amount of kaolinite and corresponding lower amount of illite (Table 16).

Table 15: Clay minerals and Figures of Merit (FOM).

Mineral	Figure of Merit					
	clean	Well 1	Well 2	Well 3	Well 4	Well 5
Kaolinite	1.457	1.285	1.22	1.065	1.426	1.766
Illite	1.814	1.617	1.881	2.242	2.937	1.845
Quartz	0.577	0.880	0.662	0.457	1.024	1.001
Vermiculite	1.254	1.504	1.267	1.582	0.900	1.723

Table 16: Clay mineral percentages from X-ray diffraction analysis.

	Minerals (percentages)			
Samples	Kaolinite	Illite	Quartz	Vermiculite
control	35.9	45.5	17.9	0.7
well 1	20.4	66.7	11.7	1.2
well 2	28.4	53.1	17.1	1.4
well 3	16.7	62.3	19.3	1.7
well 4	18.5	69.6	10.7	1.2
well 5	14.0	68.8	16.5	0.7

Table 17: Correlation coefficient values (r) examining the relationship between soil hydrocarbon and soil mineral content.

Coefficient of Correlation (r-value)	Hydrocarbon Content
Kaolinite content	-0.873
Illite Content	0.846

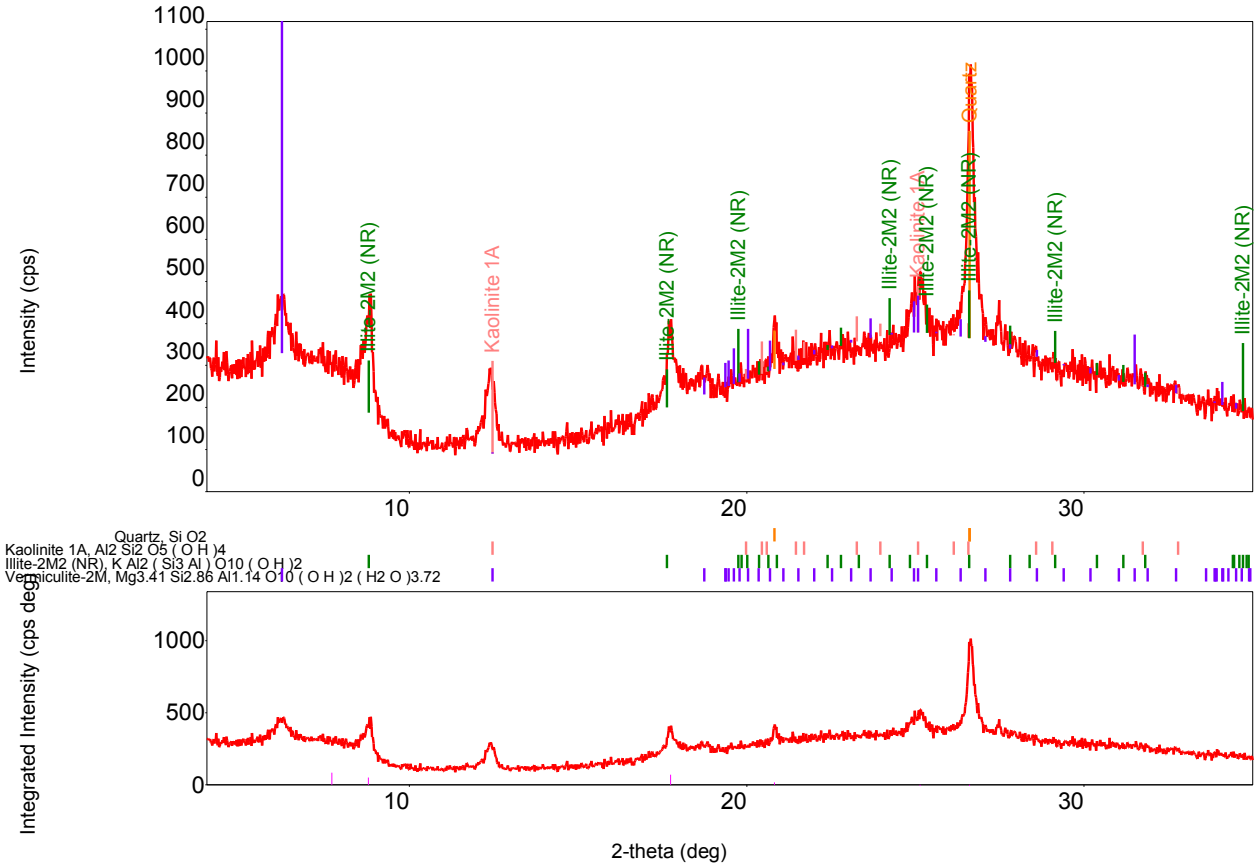

Figure 12: Control sample X-ray diffractograms for clay mineral analysis.

Table 18: Location and d-spacings for control sample diffractograms. D-spacings are given in angstroms.

No.	2-theta (deg)	d (ang.)	Height (cps)
1	6.26	14.11	94.15
2	7.70	11.47	27.09
3	8.79	10.06	141.55
4	12.4	7.13	127.53
5	17.74	4.99	113.83
6	20.83	4.26	114.74
7	25.14	3.54	79.21
8	26.61	3.35	488.07

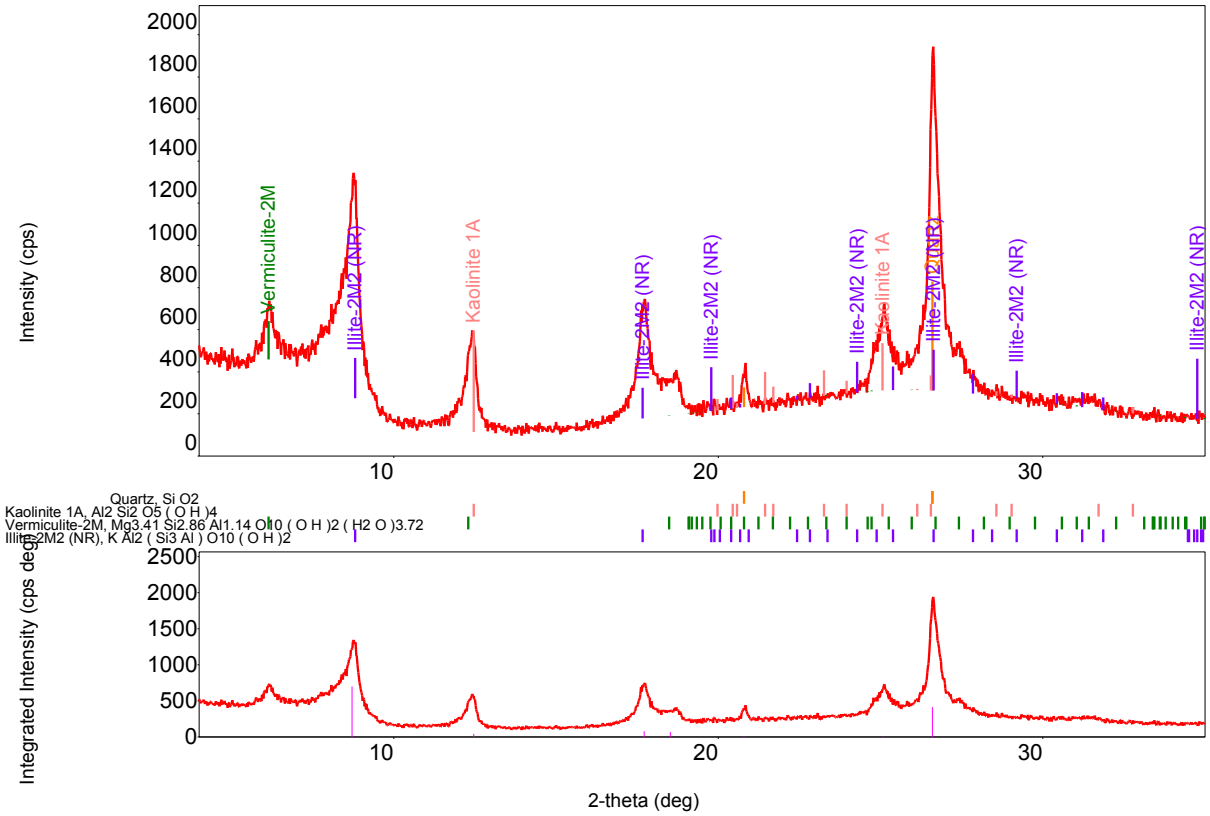

Figure 13: Well 1 X-ray diffractograms for clay mineral analysis.

Table 19: Location and d-spacings for well 1 diffractograms. D-spacings are given in angstroms.

No.	2-theta (deg)	d (ang.)	Height (cps)
1	6.14	14.39	127.41
2	8.71	10.14	619.85
3	12.47	7.09	282.91
4	17.72	5.00	281.8
5	18.52	4.79	114.53
6	20.79	4.27	125.24
7	25.07	3.55	202.19
8	26.59	3.35	1035.65

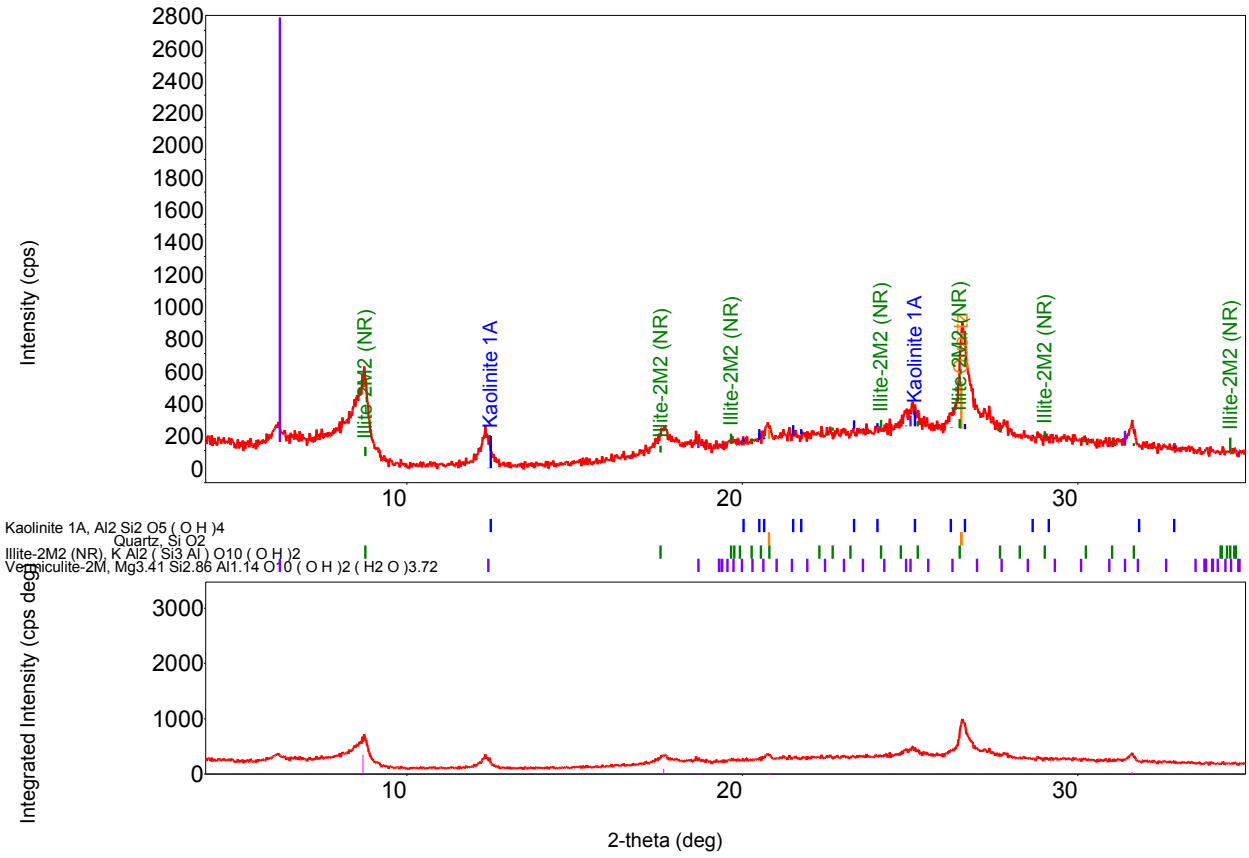

Figure 14: Well 2 X-ray diffractograms for clay mineral analysis.

Table 20: Location and d-spacings for well 2 diffractograms. D-spacings are given in angstroms.

No.	2-theta (deg)	d (ang.)	Height (cps)
1	6.20	14.24	72.81
2	8.69	10.17	296.06
3	12.34	7.17	147.27
4	17.66	5.02	87.28
5	18.70	4.74	67.28
6	20.79	4.27	84.5
7	25.14	3.54	104.27
8	26.52	3.36	431.45
9	31.62	2.83	110.17

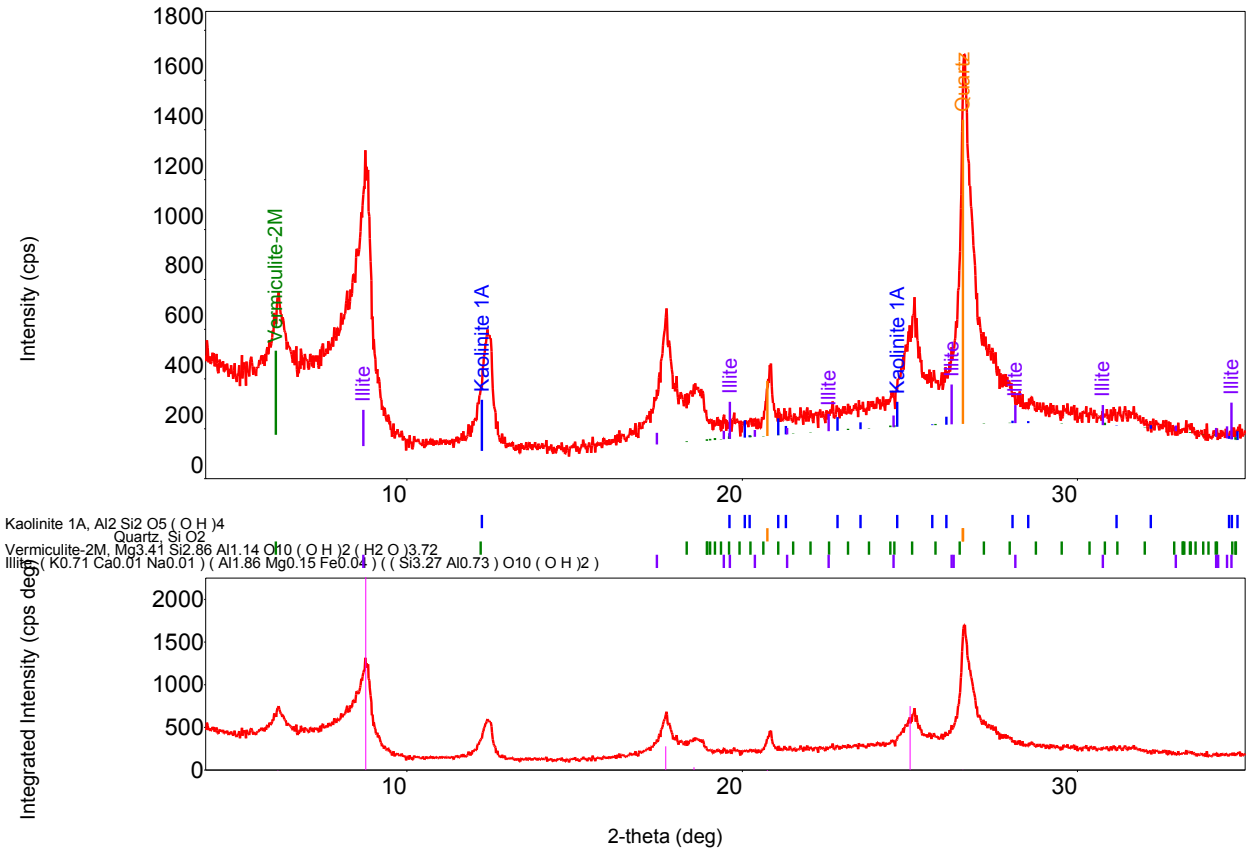

Figure 15: Well 3 X-ray diffractograms for clay mineral analysis.

Table 21: Location and d-spacings for well 3 diffractograms. D-spacings are given in angstroms.

No.	2-theta (deg)	d (ang.)	Height (cps)
1	6.15	14.36	248.99
2	8.77	10.07	518.44
3	12.44	7.11	319.58
4	17.72	5.00	309.48
5	18.56	4.77	109.37
6	20.76	4.28	119.02
7	25.00	3.56	194.81
8	26.58	3.35	1029.55

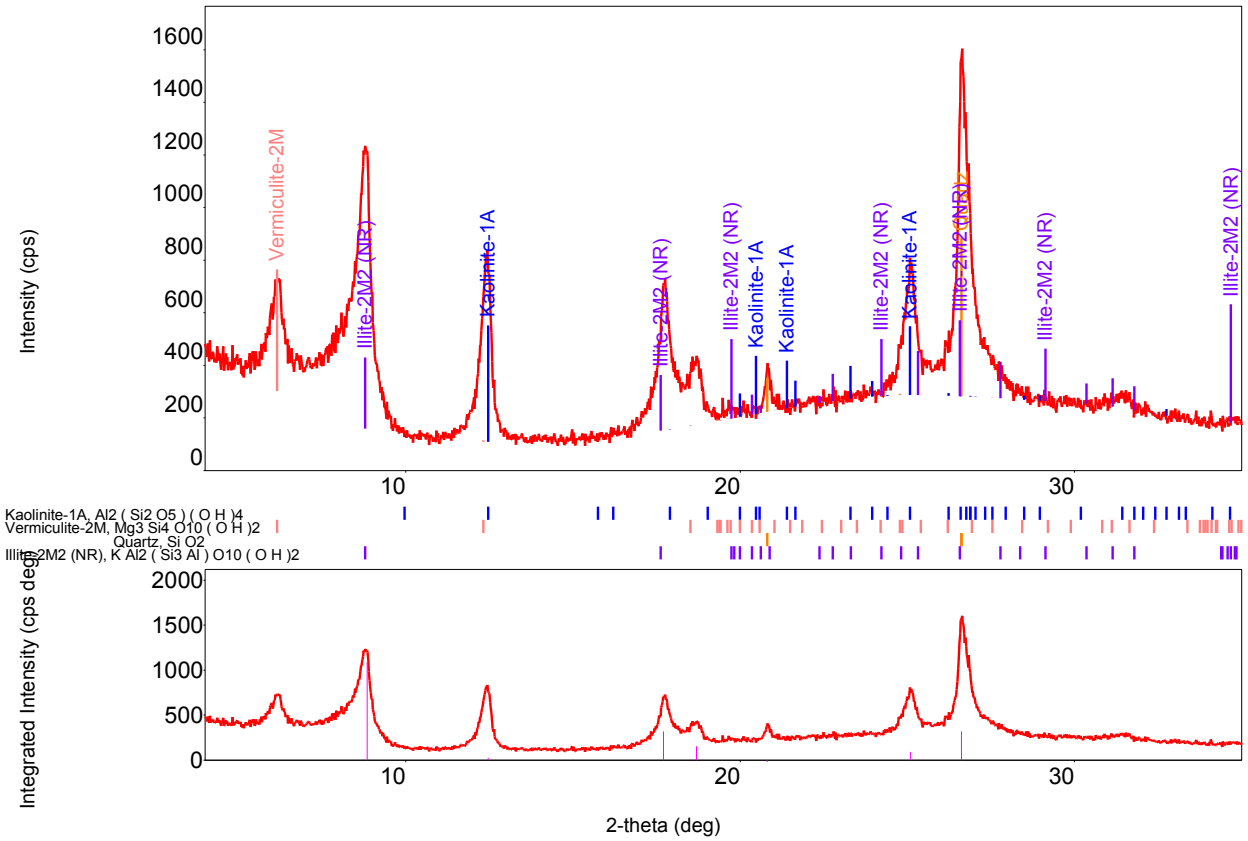

Figure 16: Well 4 X-ray diffractograms for clay mineral analysis.

Table 22: Location and d-spacings for well 4 diffractograms. D-spacings are given in angstroms.

No.	2-theta (deg)	d (ang.)	Height (cps)
1	6.15	14.35	246.18
2	8.84	9.99	685.65
3	12.46	7.098	457.35
4	17.71	5.00	359.01
5	18.69	4.74	152.1
6	20.81	4.26	119.45
7	25.09	3.55	305.6
8	26.62	3.35	844.57

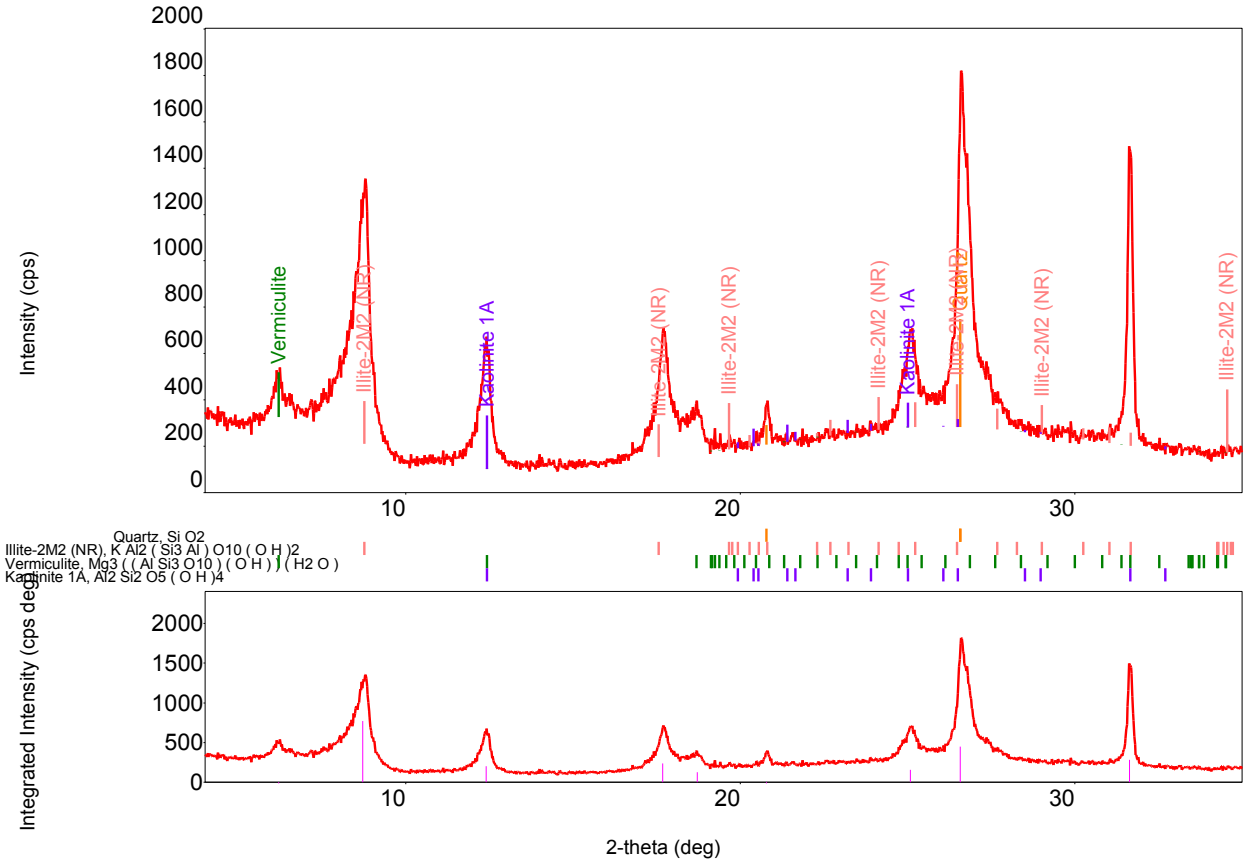

Figure 17: Well 5 X-ray diffractograms for clay mineral analysis.

Table 23: Location and d-spacings for well 5 diffractograms. D-spacings are given in angstroms.

No.	2-theta (deg)	d (ang.)	Height (cps)
1	6.20	14.24	138.58
2	8.71	10.14	680.14
3	12.41	7.13	364.13
4	17.68	5.01	348.44
5	18.72	4.74	113.03
6	20.79	4.27	136.04
7	25.08	3.55	237.66
8	26.58	3.35	997.2
9	31.63	2.83	1109.36

.

Soil Temperature Analysis

In almost all of the sites, the surface temperature is decreasing with distance from the wells. Thermal images measuring surface temperature of the soil surrounding the wells can be observed in Figures 18 – 21. The difference in temperature is observed between the areas close to the well and areas 5 m from the wells. Soil surface temperatures next to the wells have an average temperature of 23.06 ^{0}C while surface temperatures located farther away have an average temperature of 20.9 ^{0}C (Table 24). Soil around wells 2 and 3 had the highest surface temperature of all the wells. Well 5 had the greatest temperature difference between soil directly next to the well and soil located farther away. A statistically significant difference exists between soil temperatures close to the well and soil temperatures a little over a meter from the well. Wells 3 (Figure 20) and 5 (Figure 21) clearly shows a thermal gradient decreasing with distance from the well. Surface temperature readings taken at 5 m from the wells are similar to those found 1 m from the well. This indicates that hydrocarbons are located close to the wells.

There is a strong correlation between the surface temperature data and the soil hydrocarbon content ($r= 0.844$) (Table 25). It is obvious on the thermal images that where hydrocarbons are present, the soil temperatures is higher. However, no conclusions can be drawn about the correlation between soil temperature and hydrocarbon content beyond 1 m from the well as the lab testing for hydrocarbon content was limited.

Table 24: Average soil surface temperature of soil directly next to wells versus 5 m from wells.

	Average temperatures		
Well	At well (^{0}C)	Away from well (^{0}C)	Difference (^{0}C)
1	22.7	20.1	2.6
2	23.62	21.58	2.04
3	23.62	21.45	2.17
5	22.12	19.41	2.71
Overall	23.06	20.9	

Table 25: Correlation coefficient values (r) examining the relationship between soil hydrocarbon content and surface temperature

Coefficient of Correlation (r-value)	Hydrocarbon Content
Surface Temperature	0.844

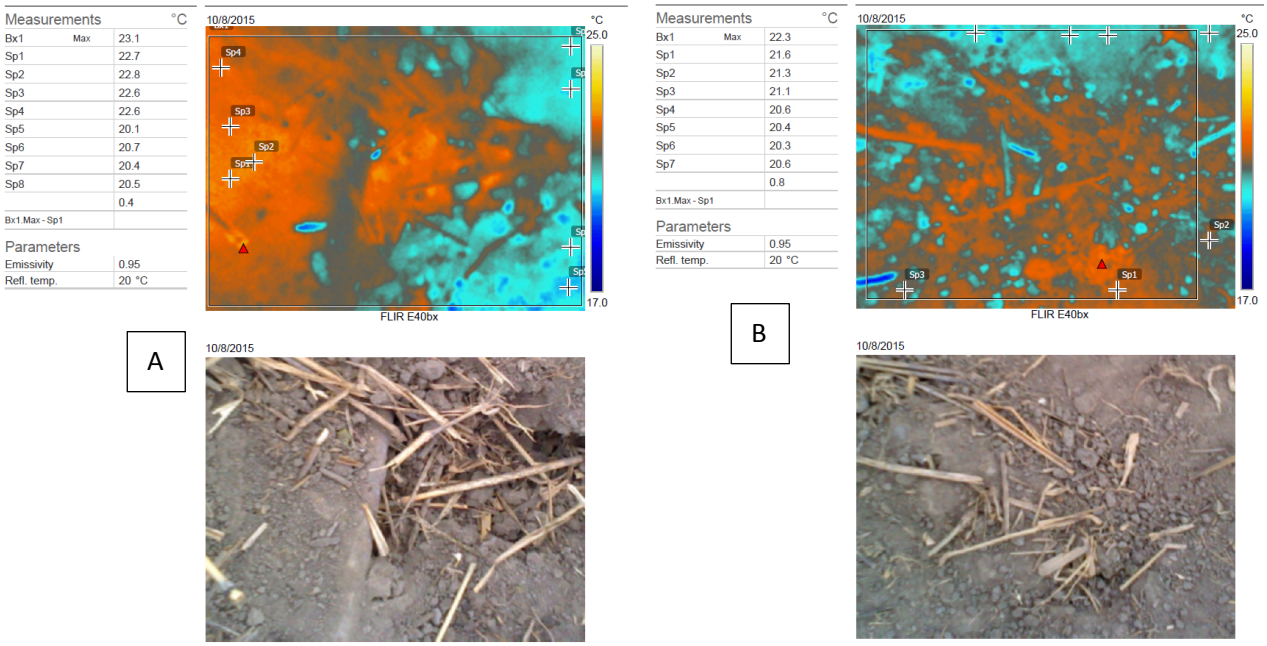

Figure 18: Thermal infrared images of soil at Well 1 showing surface temperature. (A) Well 1 thermal image (top) and digital image (bottom) at the well. Well is located just off camera to the left of the image. (B) Well 1 thermal image (top) and digital image (bottom) taken 5 m from the well. Image scale is about 1 m.

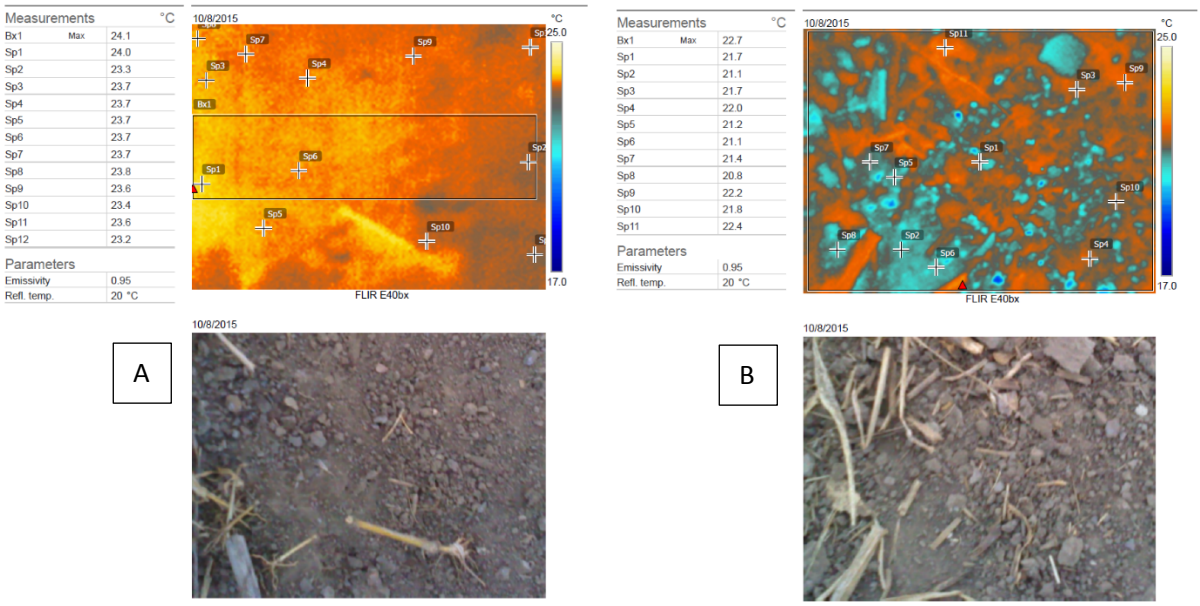

Figure 19: Thermal infrared images of soil at Well 2 showing surface temperature. (A) Well 2 thermal image (top) and digital image (bottom) taken at the well. Well is located just off camera to the left of the image. (B) Well 2 thermal image right (top) and digital image (bottom) taken 5 m away from well. Image scale is about 1 m.

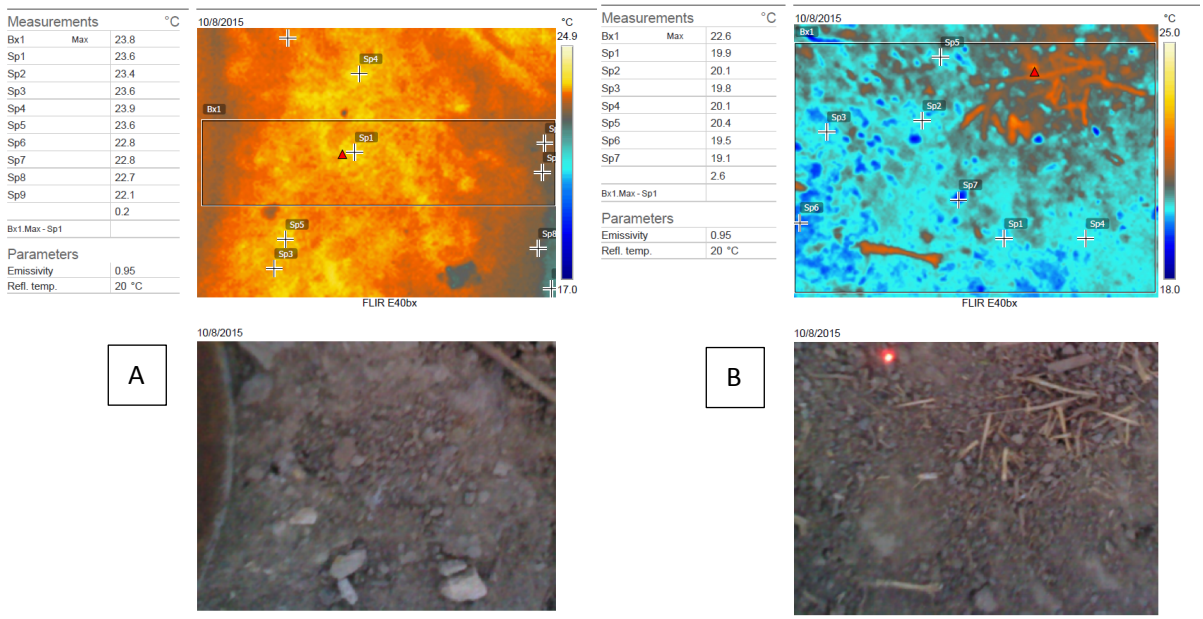

Figure 20: Thermal infrared images of soil at Well 3 showing surface temperature. (A) Well 3 thermal image right (top) and digital image (bottom) taken at the well. Part of well casing is visible on left side of image. Note the thermal gradient ring mirroring the shape of the well. (B) Well 3 thermal image right (top) and digital image (bottom) taken 5 m from the well. Red dot in image is thermal camera laser sighting. Image scale is about 1 m.

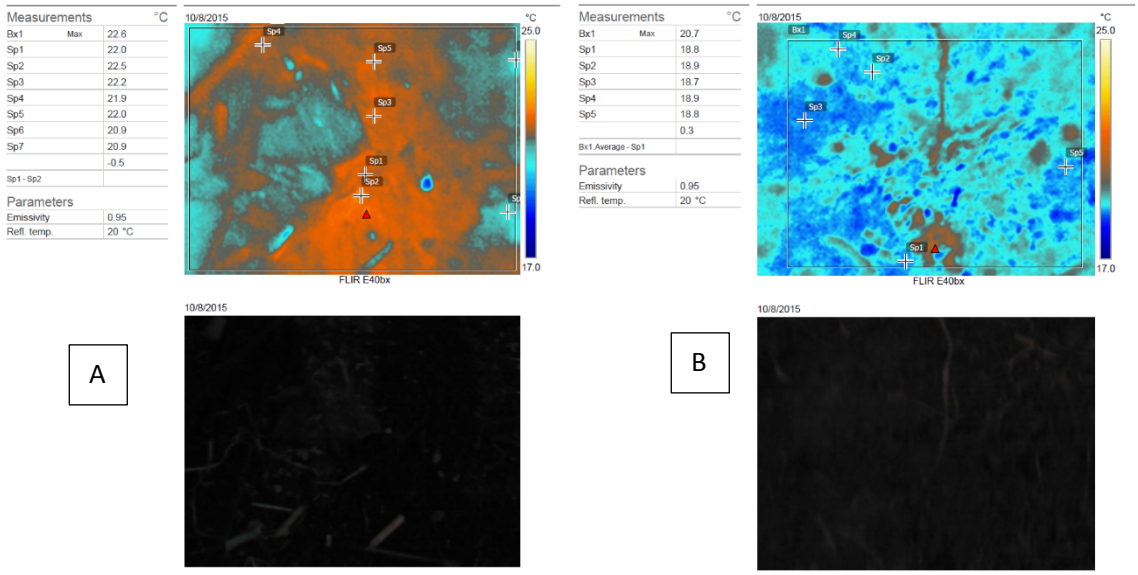

Figure 21: Thermal infrared images of soil at Well 5 showing surface temperature. (A) Well 5 thermal image (top) and digital image (bottom) taken at the well. Well is located just off camera to the left of the image. (B) Well 5 thermal image right (top) and digital image (bottom) taken 5 m away from well. Image scale is about 1 m.

Landsat-8 and WorldView-3

The data gathered from the Landsat-8 image is inconclusive. As seen in the Appendix, the various indices do not show any difference between the well and the surrounding area. The large spatial resolution of the image could not identify any differences between pixels containing wells versus pixels without any wells.

The results of the WorldView-3 multispectral index (SWIR 6 / SWIR 8), simulated by spatially aggregating hyperspectral measurements, are shown in Tables 27-31. The multispectral index values of the composite measurement (combining measurements taken at 1 m and 3 m to simulate the spatial resolution of WorldView-3, referred to as 1+3 m measurements) are higher than the >30 m measurements, which was found to be statistically significant (Table 2). The WorldView-3 spectral aggregate index shows that the average index values for the 1+3 m is greater (overall average values: 1.058) while the >30 m values are generally lower (overall average values: 1.034). Wells 3, 4, and 5 have the highest average index values for the 1+3 m measurements (averages: 1.061, 1.066, 1.065 respectively). The soil hydrocarbon content for the three wells are similar to each other (Table 1), and their index values seem to indicate that (Tables 29, 30, and 31 respectively). Well 2 is again different from the other wells, having higher multispectral index values in distances beyond 30m than within the 1+3 m distance from the well (Table 28). Well 2 has the highest soil hydrocarbon content around (for the October collection date; Table 1) yet the 1+3 m measurements are still lower than the > 30 m index values. The west, south, and north index values beyond 30 m are relatively high compared to the other wells greater than 30 m index values. This could possibly indicate that the contamination is present in the area far from well 2. When well 2 is excluded from the calculations, a strong correlation (r^2= 0.831) between the hydrocarbon content and the multispectral index value is observed (Table

26). Somewhat smaller but still relatively strong, the r^2 value (0.635) is observed when well 2 is considered in the correlation. The difference between r^2 values is significant (Table 2). This may indicate that the spatial resolution of WorldView-3 is capable of differentiating soil with higher hydrocarbon content.

Table 26: Coefficient of determination values (r^2) examining relationship between soil hydrocarbon content and WorldView-3 multispectral index values.

Coefficient of determination (r^2 values)	Hydrocarbon Content (without well 2 included)	Hydrocarbon Content (with well 2 included)
Multispectral Index	0.831	0.635

Table 27: Well 1 multispectral index values (SWIR 6 / SWIR 8).

WorldView-3 index	East		West		South		North	
>30 m	1.011		1.026	1.030	1.057	1.023	1.046	1.019
3 m	1.005	1.017	1.015	1.019	1.041	1.035	0.987	0.993
1 m	1.095	1.05	1.109	1.068	1.110	1.088	1.060	1.067
1+3 m	1.050	1.034	1.062	1.044	1.076	1.061	1.023	1.030
Average (>30 m)	1.011		1.028		1.040		1.033	
Average (3 m)	1.012		1.017		1.038		0.990	
Average (1 m)	1.073		1.089		1.099		1.063	
Average (1+3 m)	1.042		1.053		1.069		1.027	
Overall average (>30 m)	1.03	Standard Deviation	0.0362					
Overall average (3 m)	1.014	Standard Deviation	0.0187					
Overall average (1 m)	1.081	Standard Deviation	0.0229					
Overall average (1+3 m)	1.047	Standard Deviation	0.39					

Table 28: Well 2 multispectral index values (SWIR6/SWIR8).

WorldView-3 index	East		West		South		North	
>30 m	0.992	1.022	1.099	1.096	1.066	1.083	1.065	1.050
3 m	1.036	1.016	1.017	1.013	1.084	1.092	1.071	0.998
1 m	1.042	1.038	1.032	1.035	1.086	1.086	1.075	1.073
1+3 m	1.039	1.027	1.025	1.024	1.085	1.089	1.073	1.035
Average (>30 m)	1.007		1.098		1.074		1.057	
Average (3 m)	1.026		1.015		1.088		1.034	
Average (1 m)	1.040		1.033		1.086		1.074	
Average (1+3 m)	1.033		1.024		1.087		1.054	
Overall average (>30 m)	1.059	Standard Deviation	0.0369					
Overall average (3 m)	1.041	Standard Deviation	0.0362					
Overall average (1 m)	1.058	Standard Deviation	0.0236					
Overall average (1+3 m)	1.05	Standard Deviation	0.0294					

Table 29: Well 3 multispectral index values (SWIR6/SWIR8).

WorldView-3 index	East		West		South		North	
>30 m	1.028	1.016	1.041	1.017			1.044	1.062
3 m	1.044	1.039	1.044	1.058	1.043	1.039	1.137	1.085
1 m	1.028	1.016	1.075	1.095	1.071	1.070	1.052	1.076
1+3 m	1.036	1.027	1.060	1.077	1.057	1.055	1.094	1.080
Average (>30 m)	1.022		1.029		1.103		1.053	
Average (3 m)	1.041		1.051		1.041		1.111	
Average (1 m)	1.022		1.085		1.071		1.064	
Average (1+3 m)	1.032		1.068		1.056		1.088	
Overall average (>30 m)	1.035	Standard Deviation	0.0176					
Overall average (3 m)	1.061	Standard Deviation	0.0344					
Overall average (1 m)	1.06	Standard Deviation	0.0268					
Overall average (1+3 m)	1.061	Standard Deviation	0.0229					

Table 30: Well 4 multispectral index values (SWIR6/SWIR8).

WorldView-3 index	East		West		South		North	
>30 m	1.038	1.004	0.994	0.988	1.007	1.018	1.017	1.004
3 m	1.074	1.061	0.986	0.999	1.099	1.095	1.111	1.072
1 m	1.114	1.080	1.031	1.022	1.083	1.088	1.062	1.085
1+3 m	1.094	1.070	1.008	1.011	1.091	1.092	1.086	1.078
Average (>30 m)	1.021		0.991		1.012		1.010	
Average (3 m)	1.068		0.993		1.097		1.091	
Average (1 m)	1.097		1.027		1.085		1.073	
Average (1+3 m)	1.082		1.010		1.091		1.082	
Overall average (> 30m)	1.009	Standard Deviation	0.0156					
Overall average (3 m)	1.062	Standard Deviation	0.046					
Overall average (1 m)	1.071	Standard Deviation	0.0308					
Overall average (1+3 m)	1.066	Standard Deviation	0.0384					

Table 31: Well 5 multispectral index values (SWIR6/SWIR8).

WorldView-3 index	East		West		South		North	
>30 m	1.008	1.046	1.032	1.021	1.081	1.004	1.040	1.034
3 m	1.023	1.039	1.004	1.015	1.080	1.017	1.064	1.038
1 m	1.055	1.043	1.069	1.113	1.148	1.142	1.095	1.099
1+3 m	1.039	1.041	1.036	1.064	1.114	1.080	1.080	1.068
Average (>30 m)	1.027		1.026		1.043		1.037	
Average (3 m)	1.031		1.009		1.049		1.051	
Average (1 m)	1.049		1.091		1.145		1.097	
Average (1+3 m)	1.040		1.050		1.097		1.074	
Overall average (>30 m)	1.033	Standard Deviation	0.0242					
Overall average (3 m)	1.035	Standard Deviation	0.0262					
Overall average (1 m)	1.096	Standard Deviation	0.0386					
Overall average (1+3 m)	1.065	Standard Deviation	0.0288					

DISCUSSION

Landsat-8 and WorldView-3 Spectral Aggregation

As this study's attempt to detect the abandoned oil wells using Landsat-8 is unsuccessful, the study concentrates on the in situ hyperspectral data. Spatial resolution of the Landsat imagery is the main obstacle to monitor small abandoned wells. Based on the results from several measurement approaches, the soil contamination extends only a few meters from the well, therefore losing the spectral response in the 30 m x 30 m pixel. Hydrocarbons are not detected spectrally outside of the 3 m measurement distance and the target area is small in comparison to the pixel's footprint. Several studies used Landsat to detect mineral and rock alterations caused by anomalous hydrocarbon concentrations, but these studies had larger areas of contamination. Almeida-Filho et al. (2002) used Landsat 5 TM to identify anomalous hydrocarbon concentrations in soil by creating a false color composite image using band ratios of bands 2, 3, and 4 (band 2 / band 3 (R), band 4 / band 3 (G), and [band 2 / band 3]- [band 4 / band 3] (B)). This band math combination led to a tonal anomaly in the image, which was identified to be over an area of increased soil hydrocarbons. In another study, Zhang et al. (2009) used Landsat 7 Enhanced Thematic Mapper to identify heavy oil in Songliao Basin, China. False color composite images using band 4/ band 3 (ferrous iron represented by low value), band 3/ band 1 (bleaching of red beds represented by low value) and band 7/ band5 (clay mineral and carbonate represented by low value) led to the identification of regions with anomalous readings and identification of areas with increased hydrocarbon content. Borton (2007) conducted a similar study in the same area as this study using ASTER in conjunction with field spectral data. She also found that the coarse spatial resolution of ASTER does not allow it to be used for identifying individual oil wells, similar to Landsat-8.

Worldview-3 has a superior spatial resolution compared to Landsat-8, with 1.24m and 3.7m resolution in VNIR and SWIR respectively, which could be useful to identify hydrocarbon contamination from small wells. A study done by Asadzadeh and Souza Filho (2016) found that bands 9 (1.195-1.225 μm), 12 (1.710-1.750 μm), and 16 (2.295-2.365 μm) were suitable for detecting hydrocarbons. They determined that band 12 was ideal because it had bands on either side which could be used to create a simple index of [(band 11 + band 13) / band 12], which would highlight the presence of hydrocarbons in an area (Asadzadeh and Souza Filho, 2016).

This study confirms that simulated WorldView-3 spectral bands generated by the spectral aggregation of in situ hyperspectral measurements is capable of detecting the hydrocarbon absorption feature at 2.3 μm by creating an index using SWIR bands 6 and 8. The multispectral index that simulated the WorldView-3 bands suggests that WorldView-3 could be an optimal sensor for detecting the hydrocarbon features for small wells. SWIR Bands 6 and 8 can be used to detect the changes in the spectral signature around the hydrocarbon absorption feature. However, it is important to mention that the contamination would be observed within only one pixel in cases of small contaminations. Thus, different analytical approaches should be incorporated to avoid misclassification of these pixels where values could be caused by different anomalies. In addition, buried wells are likely to have a much more diffuse surface expression than those wells visible on the surface. The hydrocarbons might be present but more spread out and in lower concentrations. The spatial resolution of WorldView-3 is ideal for locating abandoned wells compared to other available multispectral sensors but more data is needed to conclude if diffuse targets like buried wells could be identified. It is suggested that spectral signatures of crops should be incorporated in the analysis.

In Situ Hyperspectral and Thermal Field Measurements

The distinctive spectral regions used to derive the index values in this study coincide with findings in the literature. The region used in this study's analysis does not include water absorption bands at 1.4 μm and 1.9 μm, as these bands are characterized in the literature but rather concentrate on the far infrared spectral range.

In this study, the statistical correlation between the hydrocarbon content and both the slope values (r = -0.596) and hyperspectral index values (r = 0.862) agrees with the findings in the literature (Cloutis, 1989; Leifer et al., 2006). The r^2 values for the slope analysis were 0.356, suggesting that prediction of the hydrocarbon content based on the slope analysis of the in situ hyperspectral measurements cannot be used with certainty. However, the strong r^2 values between soil hydrocarbon content and the hyperspectral index values (0.743) indicates that this relationship may be more reliable to predict soil hydrocarbon content. However, more data are needed to support the statistical conclusions in this study.

The hydrocarbon content results from the EPA 8015 test show that within the 1 m distance, the levels of hydrocarbons in the soil were many times greater than that of the rest of the study site. Yang et al. (1998) conducted a study on the effects of hydrocarbon microseepages where they found absorption features at 1.72 μm, 1.76 μm, 2.310 μm, and 2.330 μm, which are close to that of crude oil. The first two features were not observed in the spectral data gathered in this study but changes in the 2.3 μm region were present. The author also indicated that several clay minerals that are common to hydrocarbon altered soils (kaolinite, illite, and calcite) have spectral absorptions bands in the same wavelengths (2.2 μm-2.4 μm). Similar results were found in other studies (Cloutis, 1989; Leifer et al., 2006; Nawar et al., 2016). According to the soil survey done for the Hoytville clay loam performed by Blevins and Wilding (1968), the soil

contained on average 5.6 percent calcium carbonates. Carbonate minerals have a moderately strong spectral feature around 2.3 μm (Gaffey, 1987), but no carbonate minerals were observed in this study's XRD tests consequently their influence on the spectral reflectance is unknown.

In this study, the results of the hyperspectral reflectance measurements of the clay minerals in the clay sized fraction soil samples seem to indicate that changes in clay mineralogy do not affect the 2.3 μm region as much as hydrocarbons. The variations in the illite and kaolinite contents did not lead to any statistically significant changes in the multispectral index values calculated for the region compared to the multispectral index values calculated for the in situ soil located far from the well.

In other studies, the same spectral region was examined for other possible soil components. For example, it was found that nitrogen (N), phosphorus (P), organic carbon (OC), organic matter (OM), and iron minerals (Fe), do not affect the region around 2.3 μm (P: 0.869 μm; N: 1.702, 1.87, 2.052 μm; OC: 1.744, 1.870, 2.052 μm; OM: 0.5-1.2 μm; Fe: around 1.0 μm) (Matthews et al., 1973; Dalal and Henry, 1986; Ben-Dor, 2000; Bogrecki and Lee, 2005. Some of these studies rather suggested that the change in the spectral signature around 2.3 μm is caused by a combination of bitumen and methane.

The slope and index analysis in this study indicate that as the levels of hydrocarbons increases, the slope increases at different rates, leading to a higher index value. With the exception of well 2, where the index value is higher at 30 m than at the well, the rest of the wells are in agreement. It is unknown why well 2 is different from the other wells. There is a possibility that another unreported well could be nearby is influencing the readings. Another reason for the anomaly can be related to errors during the measurement with the hyperspectral spectroradiometer. A third possibility is that because the farm plots in the area are tiled (water

drainage systems buried beneath the surface to channel excess water to drainage ditches), the hydrocarbons could travel along the tiles away from the well. Where there is a break in the tile, hydrocarbons can then percolate up to the surface, possible some distance from the actual well location. This can also suggest some random contamination, most likely due from some leaks from oil storage and well blow-outs from the original drilling (Rarick, 1980).

When correlated with the hydrocarbon content ($r^2 = 0.743$), the hyperspectral index indicates that the linear regression model can be used for the prediction of hydrocarbon content based on the multispectral index. More data would be necessary to support the conclusion about the linearity, though it is anticipated that based on the strong correlation coefficient between soil hydrocarbon content and the hyperspectral index values ($r = 0.862$), more data would most likely strengthen the relationship.

Four out of the five wells displayed surface temperature differences where higher temperatures were observed near wells and lower temperatures were observed 5 m from the wells. Higher temperatures near the wells in this study agree with other studies, which shows that temperatures are higher in areas with hydrocarbon contamination (Nasipuri et al., 2006; ud din et al., 2008). Hydrocarbons have a much lower heat capacity then water (heavy oil: 1.67-2.09 kJ/kg°C and bitumen: ~1.78 kJ/kg°C versus water: 4.182 kJ/kg°C), meaning that they will change temperatures faster and have a higher temperature when exposed to the same amount of energy as water. Thermal anomalies are one of the several surface expressions of hydrocarbon microseepages as discussed in Zhenhai et al. (1999) and Schumacher (2000). They discussed that over areas that contain hydrocarbon microseepages, there is a thermal inertia anomaly, or the resistivity of materials to change in temperature. In a study of thermal inertia anomalies using

ASTER, Nasipuri et al. (2006) found that areas of hydrocarbon seepages have a higher thermal inertia than other areas.

Detection of the thermal gradients from individual wells would be difficult by satellite sensors as they usually have a large spatial resolution. For instance, the Landsat thermal bands are acquired at 100 m and even when resampled down to 30 m would be too coarse for the analysis. ASTER has a similar issue in that its thermal bands collect data in 90 m pixels, which are too large to detect temperature variations around small oil wells.

Landsat thermal data worked in other studies over larger contaminated areas. A study done by ud din et al. (2008) focused on the effects of damaged oil wells in the Burgan oil fields in Kuwait after the First Gulf War using Landsat TM thermal images. They found that higher land surface temperatures correlated with higher hydrocarbon content in the soil. Another study by Xing et al. (2015) also used Landsat thermal data (Landsat-5 TM and 7 ETM+) in examining the oil plumes from the Deepwater Horizon oil spill. These studies show it is possible to detect the temperature changes with Landsat, just not on the scale this study has been conducted.

A study by van der Meijde et al. (2013) found that it is possible to use multi-band thermal infrared camera to identify areas with higher hydrocarbon content. Their study created a model suggesting that hydrocarbons have a signature absorption feature at 10.00-12.75 μm region. They also found that thermal signatures are influenced by the type of soil. Soils with high clay content do not have absorption features in the thermal region while soils with a high quartz content have very strong features in the 10.50-12.50 μm region, making clay soils ideal for hydrocarbon detection (van der Meidje et al., 2013). This method was not explored in this study but could prove useful because of the high clay content in the soil in this study.

Hydrocarbon Content and Clay Mineral XRD Analysis

The results of the EPA 8015 ORO (oil range organics) test indicates that only long chain hydrocarbons (C 30+) are present in the soil. The lack of DRO (diesel range organics) range hydrocarbons suggests that the contamination around the wells in the study area does not originate from recent oil seepage. This further suggests that the wells may not be active or the oil is not reaching the surface. Lighter hydrocarbons (DRO range) should be present in the soils if the wells are actively leaking. From this analysis, it is suggested that the soil contamination is oil residue left on the surface during drilling of the wells. Drilling practices in the late 19th century were not as regulated as present day and oil likely spilled from the wells, holding tanks, and dump sites (Rarick, 1980). The latter can be the case for well 2 where some contamination was found far from the well. Among other factors such as agricultural tiling system (see above), leakage from holding tanks (which did not have bottoms and were made of wood) can cause the observed trend (Rarick, 1980). All lighter hydrocarbons likely degraded over time, leaving only the heavy and structurally complex hydrocarbons. In Marchal et al. (2003), they found that gasoline and diesel range hydrocarbons were mostly degraded by bacteria and microorganisms over their 28 day tests (96 percent and 60-73 percent respectively). Long chain hydrocarbons do not break down at the same rate as gasoline or diesel range hydrocarbons and are the most resistant to degradation (Atlas, 1981; Marchal et al., 2003; Olajire and Essien, 2014). The longer and more structurally complex hydrocarbons are very resistant to degradation and can remain in the soil for a long period of time (Marchal et al., 2003; Olajire and Essien, 2014). Crude oils also never completely degraded and leaves some kind of residue, often a black tar-like substance that has a large proportion of asphaltic compounds (Atlas, 1995). This description fits what was found around well 5, a black tar like substance was present in the soil and surrounding plants.

The low number of wells prevents large scale analysis but the results still have implications. The conclusions from the analysis can be used to suggest the exploration in future studies where reflectance measurements between old and more recent oil contamination should be compared to examine the source of contamination.

The reason why the soil hydrocarbon content is higher in August than in October (Table 1) is not clear. Long chain hydrocarbons are very resistant to bacterial degradation. The air temperatures were higher in August; however, it is not expected that the air temperature had an impact on the heavy hydrocarbons as they are not easily volatilized. If light hydrocarbons were present, the higher temperatures would most likely make an impact on bacteria that break down hydrocarbons in a soil environment (Venosa and Zhu, 2003).

This study found three clay minerals present in the soil samples near the wells: kaolinite, illite, and vermiculite. Illite content increases by as much as 15 percent in soil near wells compared to the control sample. This correlates well with the hydrocarbon content at each well ($r = 0.846$). Kaolinite content decreases at the wells, by as much 20 percent, compared to the control sample, leading to a strong negative correlation with hydrocarbon content ($r = -0.873$). The decrease in kaolinite concentrations at the wells compared to the control sample is interesting because usually the kaolinite content increases in hydrocarbon-induced alteration areas. Schumacher (1996) stated that hydrocarbon seepages can create an environment where stable illitic clays will alter into kaolinite, thereby increasing the kaolinite content at the expense of illite. Several other studies (Yupeng and Xuan, 2000, Yang et al., 2000, Petrovic et al., 2008) have examined the relationship of illite and kaolinite in regards to hydrocarbon seepages. Yupeng and Xuan (2000) found that illite concentrations increased in regions with high hydrocarbon content and kaolinite increased slightly. Yang et al. (2000) found that in areas

above a hydrocarbon seep, there were higher concentrations of both kaolinite and illite. In Petrovic et al. (2008), they found that in altered sandstones above hydrocarbon seepages, there was a large increase in the kaolinite content. On the other hand, Xu et al. (2008) found that in their study, illite concentrations were well above that of kaolinite in areas of hydrocarbon seepages. Not all studies explained what size fraction they were examining when conducting the XRD mineral analysis. Silt sized was the most common grain size fraction of the studies which considered grain size.

According to the soil survey of the Hoytville clay loam done by Blevins and Wilding (1968), the background kaolinite content was found to between 5 and 15 percent whereas this study found kaolinite content of 14 to 28 percent for samples taken from near the wells and 35 percent for the control site. No montmorillonite was found in the XRD analysis (as opposed to the 5 to 15 percent found in the 1968 soil survey) suggesting that the increased kaolinite percentages found in the soil samples may be substituted for the lack of montmorillonite. The vermiculite content found by the XRD is also below what is described in the soil survey (this study: 0.7-1.7 percent; soil survey: 5-15 percent). The lack of montmorillonite and low vermiculite contents could explain the high levels of kaolinite in the samples. It is important to note that there is very little in the literature that explores the rates of mineral alteration in hydrocarbon seepages. Many studies have explored the effects of long term seepages (tens of thousands of years or more) on mineral alteration but very few on short term seepages (hundreds of years) or residual oil. More research is needed into how long it takes for clay minerals to alter in environments similar to those found in areas with old hydrocarbon contamination.

The lack of sulfide minerals in also noteworthy since the oil coming from the Trenton Limestone has a very high sulfur content. At each well, there was an asphalt/rotten egg smell

coming from the wells indicating that hydrogen sulfide may be coming up to the surface. A study done by Tangestani and Validabadi (2014), which focused on hydrocarbon seepages into an evaporite formation in Iran, found several sulfur bearing minerals (alunite, natroalunite, and jarosite) in the area near the hydrocarbon seepage, which was also very high in sulfur content. It is possible that sulfur-bearing minerals are present at depth or in the surrounding bedrock (Lockport dolomite) beneath the glacial till but have not been brought to the surface soil. It is also possible that because this study focused on the clay sized fraction of the soil, there were no clay sized sulfide mineral grains or the sulfide mineral concentration was beneath detection limits (2-5 percent).

Study Uncertainties

There are some major uncertainties in this study that have to be addressed. More research with a larger number of wells is necessary to validate the conclusions of this study. The limited financing allowed for one soil sample collection per well for hydrocarbon content analysis which is not sufficient for the statistical analysis. This prevented running t-tests at different distances from the wells and identifying the causes of some of the higher index values observed in soil reflectance measurements located farther from the wells. This is particularly important for well 2, which behaved very differently from the other wells. The different behavior of Well 2 reduced the certainties of the study, especially the spectral indices values but it suggests that several factors should be considered. A circular contamination zone was assumed. Based on the behavior of well 2, this should not be the case. It is possible that the hydrocarbon surface contamination is not circular but extends in multiple directions in a non-circular fashion. More data points are necessary over a larger area (see the proposed sampling method). The effect of tiling in farmland

and hydrocarbon seepages was not explored in this study, which could affect the shape of the hydrocarbon contamination zone. Although limited in its measurements and analysis, the findings can be used to propose the sampling method when financial resources are not a limiting factor (see below).

Sampling Approach Proposed for Future Studies

More sampling locations and more hydrocarbon testing is needed to identify the exact nature and extent of the hydrocarbons in the soil around the abandoned wells. The following sampling approach is suggested for conducting hydrocarbon contamination studies of abandoned wells in Wood County, Ohio.

The collected data at locations of known wells is needed to develop the relationships between variables, which are then used to help identification of contaminated areas around unknown abandoned wells. Using at least 30-40 measurement pairs of soil hydrocarbon content and soil reflectance (indices), the correlation between these two parameters could be used to establish an algorithm that would ideally be able to predict hydrocarbon content based on soil reflectance. More measurement pairs will create a better correlation for the algorithm. This algorithm, applied to soil reflectance measurements, is used then to create a map suggesting the hydrocarbon contamination. To validate the map, at least 20 validation points in random locations would be needed to check the effectiveness and accuracy of the algorithm and estimate errors. Once the algorithm has been adjusted and perfected, it can be used in conjunction with a high spatial resolution commercial satellite (e.g. WorldView-3) to locate other areas with hydrocarbon content anomalies. A proposed sample data collection scheme is given in Figure 22.

Hydrocarbon content testing should be done at several distances from the known wells and on a more frequent basis closer to the well. More sampling close to the well will likely identify a gradient of contamination showing decreasing soil hydrocarbon content with distance from the well. This gradient trend is of particular importance for the algorithm development. Additional testing to identify what long chain hydrocarbon compounds are present in the soil would be a good approach for further research.

Hyperspectral reflectance measurements should be done in a 60 m x 60 m grid (Figure 22A) centered on the known well. Greater focus should be done on a smaller 10m x 10 m grid (Figure 22B) centered on the well with measurements taken next to the well, 1 m, 3 m, and then 5 m away. This will provide a much greater understanding of the nature of the hydrocarbon contaminated area closer to the wells. The advantages of using a grid system, unlike the cross like method used in this study, is that it would provide more data in areas that this study did not properly examine (i.e. areas not in the cardinal directions (NW, NE, SE, and SW) from the wells). Data collection should be done at least once a month from when the crops are harvested to before crops begin to sprout to consider temporal changes. This proposed method is designed for conducting measurements on soil in agricultural fields without vegetation. If a study proposes a vegetation analysis, the approach should be modified to capture vegetation reflectance at different phenological stages. Increased levels of hydrocarbons have been shown to negatively impact crop density and crop yield (Kisic et al., 2009). To examine the possibility of identifying the type of hydrocarbons (long chain versus short chain) present in the soil could be an additional component of the analysis.

Thermal imaging in this study focused on the westward direction of each well at dusk to avoid shadows cast by the well casings. However, thermal imaging should be done in a grid

fashion similar to the hyperspectral reflectance data. Thermal imaging should be focused on a 10 m x 10 m grid centered on the well (same as hyperspectral, with images taken next to the well, 1 m, 3 m, and then 5 m away; Figure 22B). The advantage of this sampling approach over the one used in this study is that it would show the extent of the temperature variations caused by hydrocarbons present in the soil and most likely detect more potential anomalies. Thermal images should also be taken at the same locations as hyperspectral reflectance measurements outside of the 10m x 10 m grid as well (Figure 22A).

For soil mineralogy determination, the silt sized fraction should be explored for XRD analysis. The Hoytville clay loam is made of approximately 40 percent silt sized sediments. Using both the silt sized fraction and the clay sized fraction of the soil will account for about 80 percent of the soil sediment, making it better suited to identify possible mineralogical changes in the soil. Using a larger grain size might reveal more minerals (pyrite, calcite, iron oxides etc.) in the soil that cannot be identified using just the clay size fraction. Mineral XRD analysis should be done on the same soil samples collected for the hydrocarbon content analysis, giving twelve samples per wells. Using this approach will help in examining the impact of hydrocarbons present in the soil on soul mineralogy in greater detail.

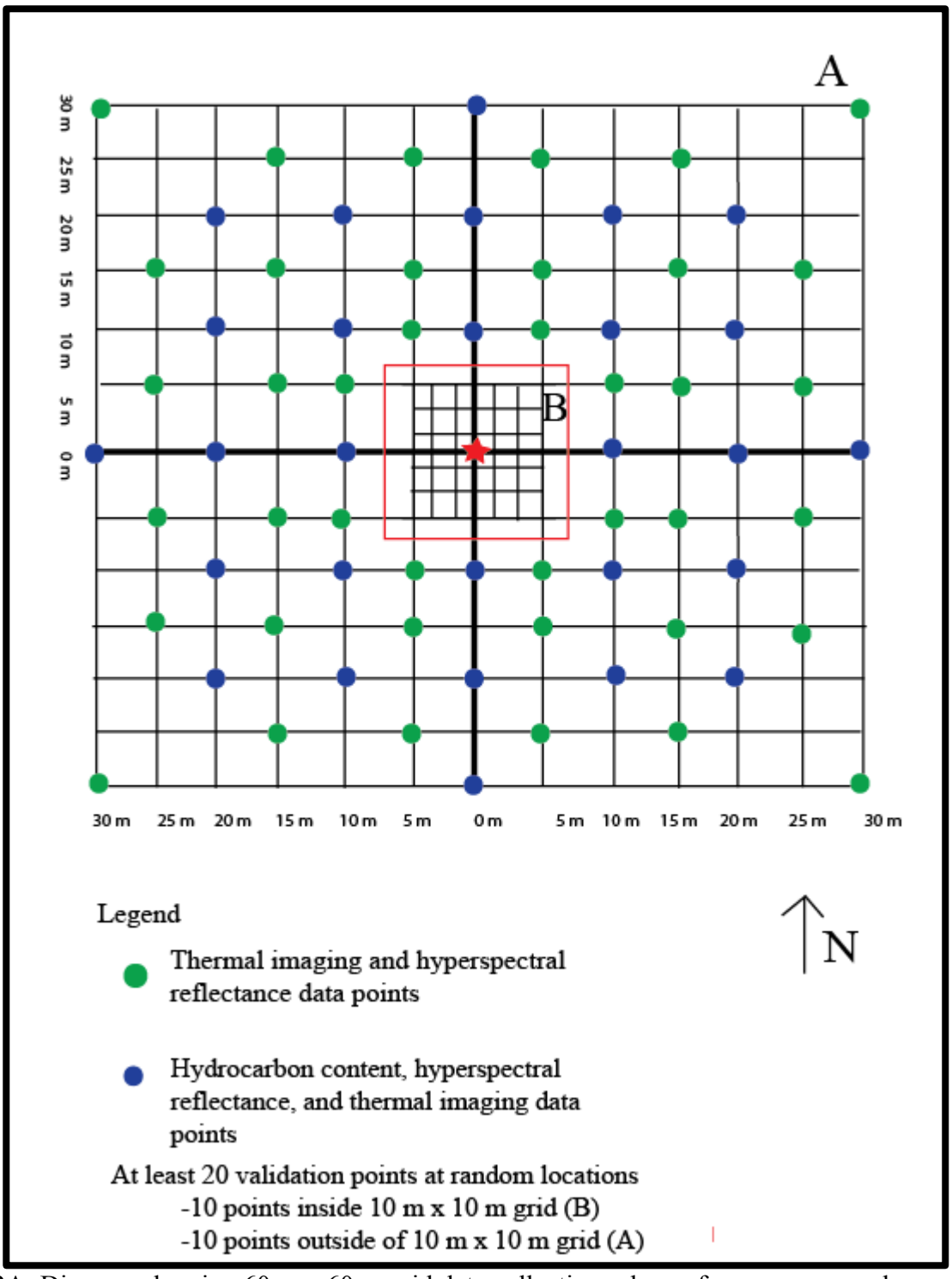

Figure 22A: Diagram showing 60 m x 60 m grid data collection scheme for new proposed sampling methods. Center 10 m x 10 m grid is shown in greater detail in Figure 22B.

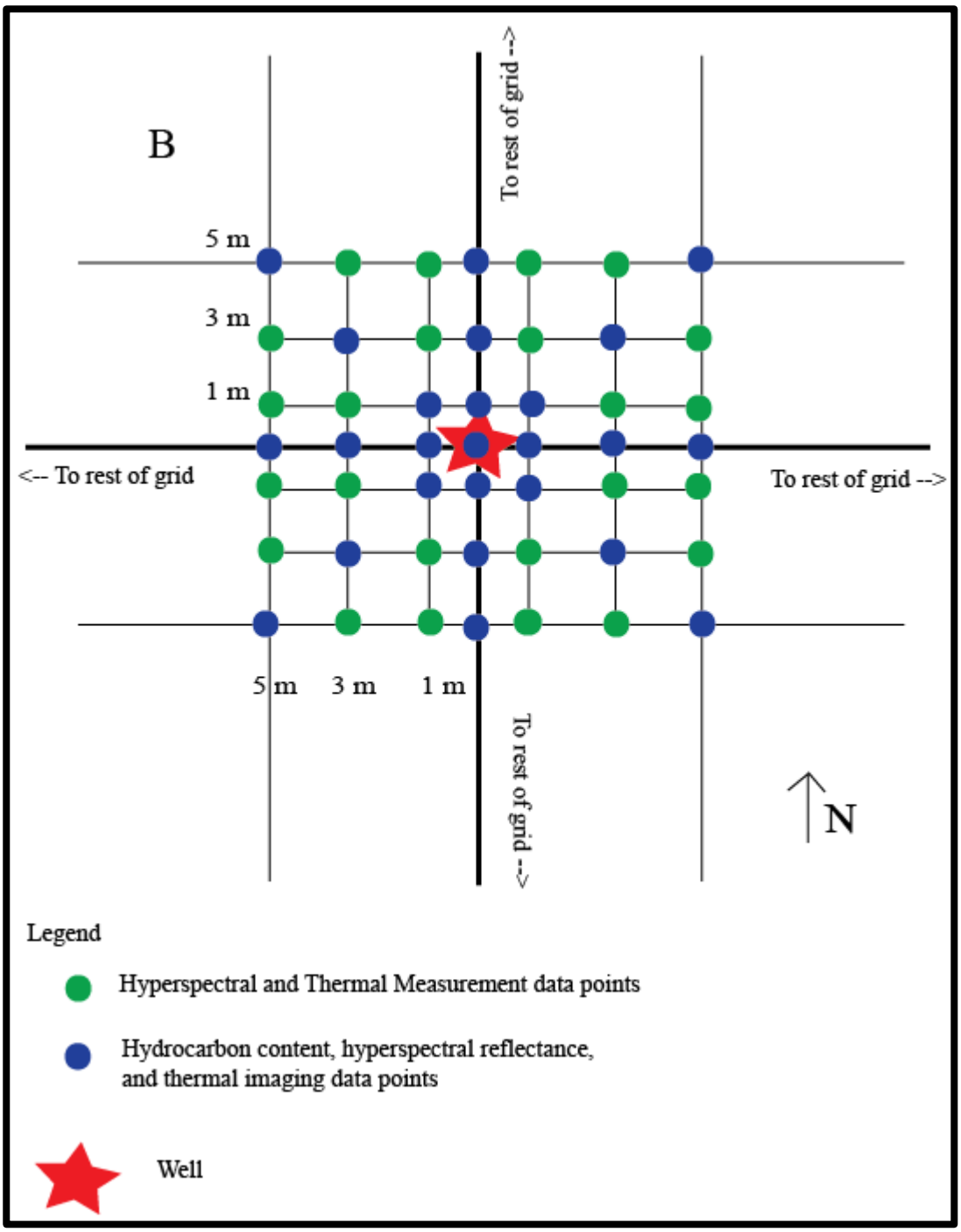

Figure 22B: Diagram showing center 10 m x 10 m grid from 60 m x 60 m grid of Figure 22A.

CONCLUSION

Detection of small abandoned wells and hydrocarbon contamination remains a problem for Wood County, Ohio. Remote sensing techniques and clay mineral XRD analysis identified changes in the soil properties that are indicative of hydrocarbon contamination. Hydrocarbon content testing determined that hydrocarbons present in the soil are not actively coming from the wells. Instead, it is likely that they are hydrocarbons left from previous spills from the drilling of the wells. Landsat-8 data proved to be inconclusive because of its coarse spectral resolution. However, the hyperspectral reflectance data using the spectroradiometer were able to detect the spectral changes in the soil caused by hydrocarbons by a slope analysis and calculating a spectral index in the 2.3μm region. The hyperspectral data also allowed for the simulating the spectral and spatial resolution of WorldView-3 bands, which was determined to be effective at identifying soil with a higher hydrocarbon content. The changes in kaolinite and illite contents in the soil as determined by the XRD analysis did not affect the spectral characteristics of the soil to the same degree as the hydrocarbons. Thermal imaging also proved effective at identifying soil surface temperature changes between soil at the wells and soil farther away.

The results of this study are by no means definitive. The low number of wells used in this study does not allow solid conclusions. The results, while not definitive, are suggestive for further research, and if given more data, they could help in future studies. The new proposed sampling approach should allow future work to examine the effects of hydrocarbons in greater detail than this study was capable of achieving. The data from this study correlates well with the low number of data points thus it is expected that more data should confirm the results of this study and strengthen the conclusions. Based on the available data, detection of abandoned wells should be possible using high spatial resolution commercial satellites (e.g. WorldView-3) in

conjunction with thermal imaging to identify areas where hydrocarbons are contaminating the soil.

REFERENCES

Almeida-Filho, A., Miranda, F.P., Galvao, L.S., and Freitas, C.C., 2002, Terrain characteristics of a tonal anomaly remotely detected in an area of hydrocarbon microseepage, Tucano Basin, north-eastern Brazil: International journal of Remote Sensing, v. 23, 3893-3898.

Asadzadeh, S., and Souza Filho, C., 2016, Investigation the capability of WorldView-3 superspectral data for direct hydrocarbon detection: Remote Sensing of Environment, v. 173, p. 162-173.

The Associated Press, 2010, 27,000 abandoned oil and gas wells in the Gulf of Mexico ignored by the government, industry: http://www.nola.com/news/gulf-oil-spill/index.ssf/2010/07/27000_abandoned_oil_and_gas_we.html (Accessed March 2016).

Atlas, R.M., 1981, Microbial degredation of petroleum hydrocarbons: an environmental perspective: Microbiological Reviews, v. 45, p. 180-209.

Atlas, R.M., 1995, Petroleum biodegradation and oil spill bioremediation: Marine Pollution Bulletin, v. 31, p. 178-182.

Ben-Dor, E., 2000, Quantitative remote sensing of soil properties: Advances in Agronomy, v. 75, p. 173-243.

Blevins, R.L., and Wilding, L.P., 1968, Hoytville soils: Their properties, distribution, management, and use: Ohio Agricultural Research and Development Center, Research Bulleetin 1006, 30 p.

Bogrecki, I., and Lee, W.S., 2005, Spectral phosphorus maping using diffuse reflectance of soils and grass: Biosystems Engineering, v. 91, p. 305-312.

Borton, T.A., 2007, Use of remote sensing and geographical techniques for locating abandoned oil wells, Wood County, Ohio [Masters thesis]: Bowling Green State University, 97 p.

Chakraborty, S., Weindorf, D.C., Morgan, C.L.S., Yufeng, G., Galbraith, J.M., Bin, L., and Kahlon, C.S., 2010, Rapid identification of oil-contaminated soils using visible near-infrared diffuse reflectance spectroscopy: Journal of Environmental Quality, v. 39, p. 1378-1387.

Cloutis, E.A., 1989, Spectral reflectance properties of hydrocarbon: remote sensing applications: Science, v. 245, p. 165-168.

Dalal, R.C., and Henry, R.J., 1986, Silmultaneous Determineation of moisture, organic carbon, and total nitrogen by near infrared reflectance spectrophotometry: Soil Science Society of America Journal, v. 50, p. 120-123.

Duncan, W.S., and Capps, R.W., 2000, Identification of hydrocarbon seeps by hyperspectral remote sensing: Gulf Coast Association of Geological Societies Transactions, v. 50, p. 75-80.

Espen, Brad, Wood County Health Department, 2015, personal communication.

Fawcett, T.G., Crowder, C.E., Kabekkodu, S.N., and Kaduk, J.A., 2011, Improved material identification methods through targeted data mining: JCPDS-International Center for Diffraction Data, ISSN 1097-0002, p. 149-161.

Gaffey, S.J., 1987, Spectral reflectance of carbonate minerals in the visible and near infrared (0.35-2.55μm): Anhydrous carbonate minerals: Journal of Geophysical Research: v. 92, p. 1429-1440.

FLIR, February 2016, FLIR Tools Software ver. 5.5 for windows, www.flir.com.

Fingas, M.F., and Brown, C.E., 1997, Review of oil spill remote sensing: Spill Science & Technology Bulletin, v. 4, p. 199-208.

Horig, B., Kühn, F., Oschutz, F., Lehmann, F., 2001, HyMap hyperspectral remote sensing to detect hydrocarbons: International Journal of Remote Sensing, v. 22, p. 1413-1422.

Jensen, J., 2006, Remote sensing of the environment: An Earth resource perspective (2nd ed): Pearson Prentice Hall, 608 p.

Johnson, S., 2015, Abandoned oil and gas wells are leaking methans across the USA: http://inhabitat.com/abandoned-oil-and-gas-wells-are-leaking-methane-across-the-usa/ (Acessed March 2016).

Kang, M., Kanno, C.M., Reid, M.C., Zhang,X., Mauzerall, D.L., Celia, M.A., Chen, Y., and Onstott, T.C., 2014, Direct measurements of methane emissions from abandoned oil and gas wells in Pennsylvania: Proceedings of the National Academy of Science, v. 111, p. 18173-18177.

Khan, S.D., Jacobson, S., 2008, Remote sensing and geochemistry for detecting hydrocarbon microseepages: GSA Bulletin, v. 120, p. 96-105.

Kisic, I., Mesic,S., Basic, F., Brkic, V., Mesic, M., Durn, G., Zgorelec, Z., amd Bertovic, L., 2009, The effects of drilling fluids and crude oil on some chemical characteristics of soil and crops: Geoderma, v. 1449, p. 209-216.

Kühn, F., Oppermann, K., and Hörig, B., 2004, Hydrocarbon index-an algorithm for hyperspectral detection of hydrocarbons: International Journal of Remote Sensing, v. 25, p. 2467-2473.

Macdonald, I.R., Guinasso, N.L., Ackleson, S.G., Amos, J.F., Duckworth, R., Sasses, R., Brooks, J.M., 1993, Natural oil-slicks in the Gulf-of-Mexico visible from space: Journal of Geophysical Research Oceans v. 98, p. 16351–16364.

Marchal, R., Penet, S., Solano-Serena, F., and Vandecasteel, J.P., 2003, Gasoline and diesel oil biodegradation: Oil and Gas Science and Technology, v. 58, p. 441-448.

Matthews, H.L., Cunningham, R.L., and Peterson, G.W., 1973, Spectral reflectance of selected Pennsylvania soils: Soil Science Society of America Journal, v. 37, p. 421-424.

McCoy, R.M., Blake, J.G., Andrews, K.L., 2001, Detecting Hydrocarbon microseepage using hydrocarbon adsorption bands of reflectance spectra of surface soils: Oil and Gas Journal, 5 p.

Moore, D.M., and Reynolds, R.C., 1997, X-ray Diffraction and the Identification and Analysis of Clay Minerals, Second Edition: New York, Oxford University Press, 378 p.

Nawar, S., Buddenbaum, H., Hill, J., Kozak, J., and Mouazen, A.M., 2016, Estimating the soil clay content and organic matter by means of different calibration methods of vis-NIR diffuse reflectance spectroscopy: Soil & Tillage Research, v. 155, p. 510-522.

Nasipuri, P., Majumdar, T.J., and Mitra, D.S., 2006, Study of high-resolution thermal inertia over western India oil fields using ASTER data: Acta Astronautica, v. 58, p. 270-278.

NEOGAP, 2009, Unplugged wells still in Wood Co.: http://www.neogap.org/neogap/2011/04/10/unplugged-oil-wells-still-in-wood-co/ (accessed February 2016)

Norris, S.E., 1975, Geologic structure near surface rocks in western Ohio: The Ohio Journal of Science, v. 75, p. 225-228.

Ohio Division of Geological Survey, 2004, Oil and gas map of Ohio: Division of Geological Survey Map PG-1, generalized page version with text, 2 p., scale 1:2,000,000.

Ohio Division of Geological Survey, 2004, Shadded drift-thickness map of Ohio: Division of Geological Survey Map SG-3, generalized page version with text, 3 p., scale 1:2,000,000.

Okparanma, N., and Mouazen, A.M., 2013, Combined effects of oil concentration, clay and moisture contents on diffuse reflectance spectra of diesel-contaminated soils: Water Air Soil Pollution, DOI 10.1007/s11270013-15398.

Olajire, A.A., and Essien, J.P., 2014, Aerobic degradation of petroleum components by microbial consortia: Journal of Petroleum and Enviornmental Biotechnology: v. 5, p. 1-22.

Onasch, C. M., and Kahle, C.F., 1991, Recurrent tectonics in a cratonic setting: An example from northwestern Ohio: Geologic Society of America Bulletin, v. 103, p. 1259-1269.

Pabón, R.E.C., and Souza Filho, C.R., 2016, Spectroscopic characterizations of red latosols contaminated by petroleum-hydrocarbon and empirical model to estimate pollutant content and type: Remote Sensing of Environment, v. 175, p. 323-336.

Petrovic, A., Khan, S.D., and Chafetz, H.S., 2008, Remote detection and geochemical studies for finding hydrocarbon-induced alterations in Lisbon Valley, Utah: Marine and Petroleum Geology, v. 25, p. 696-705.

Petrovic, A., Khan, S.D., and Thurmond, A.K., 2012, Integrated hyperspectral remote sensing, geochemical and isotopic studies for understanding hydrocarbon-induced rock alterations: Marine and Petroleum Geology, v. 35, p. 292-308

Rarick, R.D., 1980: The petroleum industry- its birth in Pennsylvania and development in Indiana: Indiana Department of Natural Resources Geological Survey Occasional Paper 32, 36 p.

Rigaku, 2011, PDXL Integrated X-ray powder diffraction software vers. 1.8.1.0, www.rigaku.com.

Robbins, R.A., and Lantz, A.M., 2007, Soil Survey of Wood County, Ohio: Ohio Department of Natural Resources, Division of Soils and Water Conservation. 1-809.

Ryan, B., 2012, Leaking old oil well to be capped at fairgrounds: http://www.sent-trib.com/community/farm/leaking-old-oil-well-to-be-capped-at-fairgrounds/article_f65bd885-35db-52e9-87b9-0d511d178fb1.html (Accessed February 2016).

Sabins, F.F., 1999, Remote sensing for mineral exploration: Ore Geology Reviews, v. 14, p. 157-183.

Schumacher, D., 1996, Hydrocarbon induced alteration of soils and sediments, *in* Shcumacher, D., and Abrams, M.A., eds, Hydrocarbon migration and its near surface expression: AAPG Memoir, v. 66, p. 71-89.

Schumacher, D., 2000, Surface geochemical exploration for oil and gas; new life for an old technology: The Leading Edge, March, 258-261.

Schwartz, G., Ben-dor, E., and Eshel, G., 2013, Quantitative assessment of hydrocarbon contamination in soil using reflectance spectroscopy: a “multipath” approach: Applied Spectroscopy, v. 67, p. 1323-1331.

Shi, P., Fu, B., Ninomiya, Y., Sun, J., and Li, Y., 2012, Multipectral remote sensing mapping for hydrocarbon seepage induced lithologic anomalies in the Kuqa forland basin, south Tian Shan: Journal of Asian Earth Sciences, v. 46, 70-77.

Smejkalova, E., and Bujok, P., 2012. Remote sensing methods in the identification of oil contaminations: GeoScience Engineering, v. 58, p. 24-33.

Spectral Evolutions Inc., 2012a, Appendix D; PSR-3500 specifications, PSR Series Spectroradiometer Operators Manuel, version 1.05, p. 27.

Spectral Evolutions Inc., 2012b, DARWin SP Application Software Version 1.2 User Manuel, version 1.2.3.5, 63 p.

Tangestani, M.H., and Khadijeh, V., 2014, Mineralogy and geochemistry of alteration induced by hydrocarbon seepages in evaporite formation; case study from Zagros Fold Belt, SW Iran: Applied Geochemistry, v. 41, p. 189-195.

ud din, S., Al Dousari, A., and Literathy, P., 2008, Evidence of hydrocarbon contamination from the Burgan oil field, Kuwait: Interpretations from thermal remote sensing data: Journal of Environmental Management, v. 86, p. 605-615.

van der Meer, F., van Dijk, P., Schetselaar, E., Little, M., Podlaha, O., Yang, H., and Biegert, E., 2000, An integrated geoscience approach for hyperspectral hydrocarbon microseepage detection, *in* Proceedings of the Thirteenth International Conference, Applied Geologic Remote Sensing, v. 4, 81-88.

van der Meer, F., van Dijk, P., van der Werff, H., and Hong Yang, 2002, Remote sensing and petroleum seepage: a review and case study: Terra Nova, v. 14, p. 1-17.

van der Meer, F.,van der Werff, H.M.A., van Ruitenbeek, F.J.A., Hecker, C.A., Bakker, W.H., Noonmen, M.F., van der Meijde, M., Carranza, E.J.M., de Smeth, J.B., and Woldai, T., 2012, Multi- and hyperspectral geologic remote sensing: A review: International Journal of Applied Earth Observational and Geoinformation, v. 14, p. 112-128.

van der Meijde, M., Knox, N.M., Cundill, S.L., Noomen, M.F., van der Werff, H.M.A., and Hecker, C., 2013, Detection of hydrcarbons in clay soils: a laboratory experiment using spectroscopy in the mid- and thermal infrared: International Journal of Applied Earth Observation and Geoinformation, v. 23, p. 384-388.

van der Werff, H.M.A., Noonmen, M.F., van der Meijde, M., Kooistra, J.F., and van der Meer, F.D., 2007, Use of hyperspectral remote sensing to detect hazardous gas leakage from

pipelines: p. 707-715 *in* Bochenek, Z. (Ed.), 2007, New Developments and Challenges in Remote Sensing: Millpress, Rotterdam, ISBN 978-90-5966-0533.

Venosa, A.D., and Zhu, X., 2003, Biodegredation of crude oil contaminating marine shorelines and freshwater wetlands: Spill Science and Technology Bulletin, v. 8, p. 163-178.

Wickstrom, L.H., Gray, J.D., and Stieglitz, R.D., 1992, Stratigraphy, structure and production history of the Trenton Limestone (Ordovician) and adjacent strata in northwestern Ohio: Columbus, Ohio Department of Natural Resources Division of Geological Survey Report of Investigation No. 143, 78 p.

Wright, P., 2012, Ohio's oil boom- why it will be different this time: Oil and Gas Law Report, http://www.oilandgaslawreport.com/2012/08/24/ohios-oil-boom-why-it-will-be-different-this-time/ (Accessed April 2016).

Xing, Q, Li, L., Lou, M., Bing, L., Zhao, R., and Li, Z., 2015, Observations of oil spills through Landsat thermal infrared imagery: a case of Deepwater Horizon: Aquatic Procedia, v. 3, p. 151-156.

Xu, D., Ni, G., Jiang, L., Shen, T., Li, T., Ge, S., and Shu, X., 2008, Exploring nor natural gas using reflectance spectra of surface soils: Advances in Space Research, v. 41. P. 1800-1817.

Yang, H., Zhang, J., van der Meer, F., and Kroonenberg, S.B., 1998, Geochemistry and field spectrometry for detecting hydrocarbon microseepages: Terra Nova, v. 10, p. 231-235.

Yatabe, S.M., and Fabbri, A.G., 1986, The application of remote sensing to Canadian petroleum exploration: Promising and yet unexplored: Computers and Geosciuences, v. 12, p. 597-609.

Yupeng, W. and Xuan, D., 2000, Hydrocarbon alteration characteristics of soils and mechanisms for detection by remote sensing in Eastern Sichuan Area, China: Natural Resources Research, v. 9., p. 295-305.

Zhang, G., Zheng, Z., Shen, X., Zou, L., and Huang, K., 2011, Remote sensing interpretation of areas with hydrocarbon microseepages in northeast China using Landsat-7/ETM+ data processing Techniques: International Jounal of Remote Sensing, v. 32, p. 6695-6711.

Zhang, G., Zou, L., Shen, X., Lu, S., Li, C., and Chen, H., 2009, Remote sensing detection of heavy oil through spectral enhancement techniques in the western slope of Songliao Basin, China: AAPG Bulletin, v. 93, p. 31-49.

Zhu, Z., and Zhang, J., 1994, Spectral remote sensing for exploring oil pools by spectral absorption bands of hydrocarbons: Proceeedings of the First International Airborne Remote Sensing Conference and Exhibition; applications, technology, and science, September 1999, v. 1, p. 514-522.

Zhenhai, Z., Xiaoxia, H., Hongmei, W., and Zhaoxiang, Q., 1999, Direct Petroleum Exploration by Using Remote Sensing Method, *in* Proceedings of the Thirteenth International Conference, Applied Geologic Remote Sensing, Vancouver, Canada, March 1999, v. 1, p. 444-451.

APPENDIX:

Table A-1: Landsat-8 band descriptions.

Bands	Band Width (μm)	Spatial resolution (m)
Band 1 Coastal aerosol	0.430-0.450	30 m
Band 2 Blue	0.450-0.510	30 m
Band 3 Green	0.530-0.590	30 m
Band 4 Red	0.640-0.670	30 m
Band 5 NIR	0.850-0.880	30 m
Band 6 SWIR 1	1.570-1.650	30 m
Band 7 SWIR 2	2.110-2.290	30 m
Band 8 Panchromatic	0.500-0.680	15 m
Band 9 Cirrus	1.360-1.380	30 m
Band 10 TIR 1	10.600-11.190	100 m
Band 11 TIR 2	11.500-12.510	100 m

Table A-2: WorldView-3 band descriptions.

Bands	Band Widths (μm)	Spatial Resolution (m)
Panchromatic	0.450-0.800	0.31
Band 1 Coastal	0.400-0.450	1.24
Band 2 Blue	0.450-0.510	1.24
Green	0.510-0.580	1.24
Yellow	0.585-0.625	1.24
Red	0.630-0.690	1.24
Red Edge	0.705-0.745	1.24
NIR 1	0.770-0.895	1.24
NIR 2	0.860-1.040	1.24
SWIR 1	1.195-1.225	3.7
SWIR 2	1.550-1.590	3.7
SWIR 3	1.640-1.680	3.7
SWIR 4	1.710-1.750	3.7
SWIR 5	2.145-2.185	3.7
SWIR 6	2.185-2.235	3.7
SWIR 7	2.235-2.285	3.7
SWIR 8	2.295-2.365	3.7

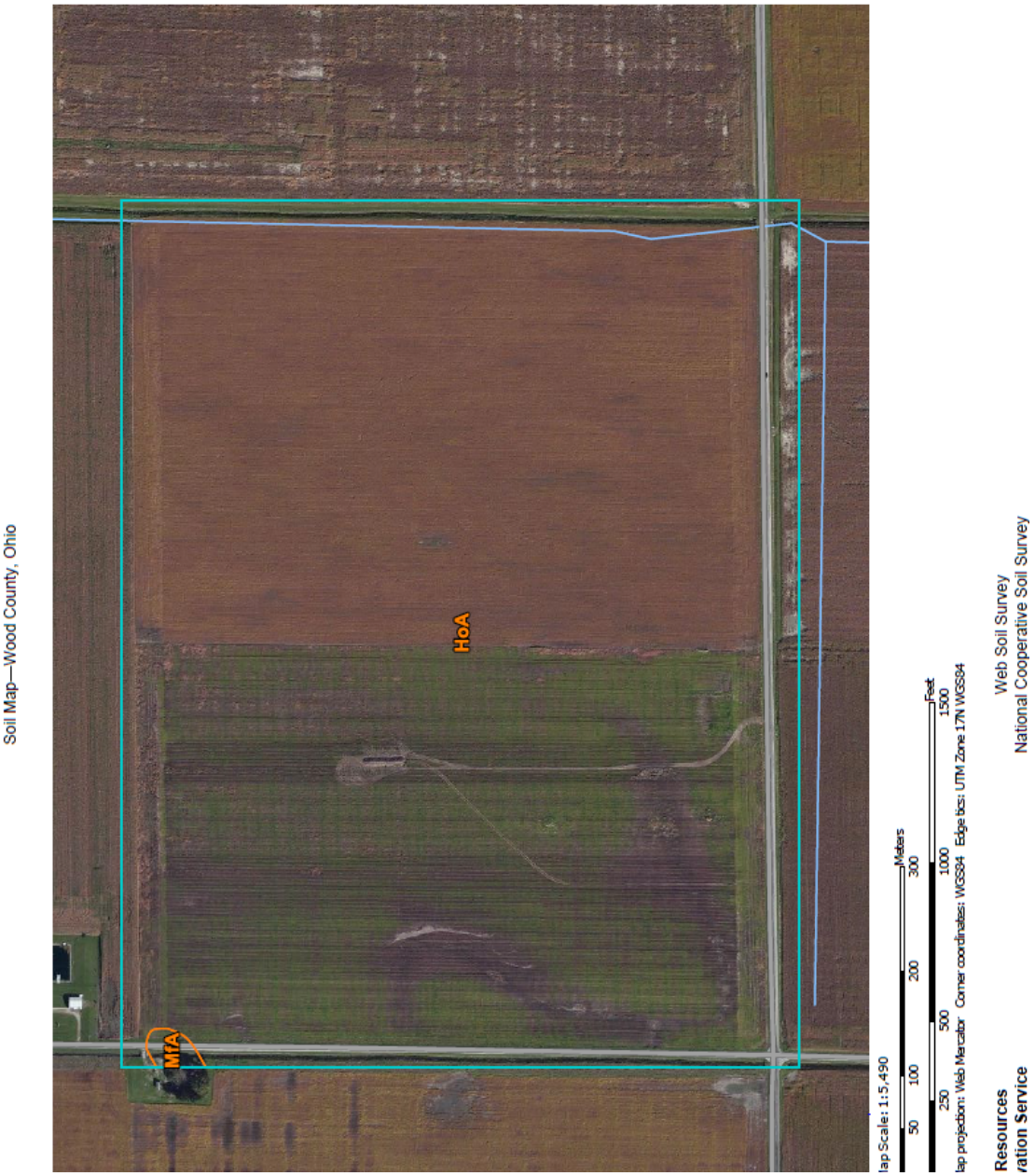

Figure A-1: Soil map of study area. Most of the plot is Hoytville clay loam (HoA), with a small amount of Mermill-Aurand complex (MfA) in the northwest corner of the plot. (From ODNR Soil Survey).

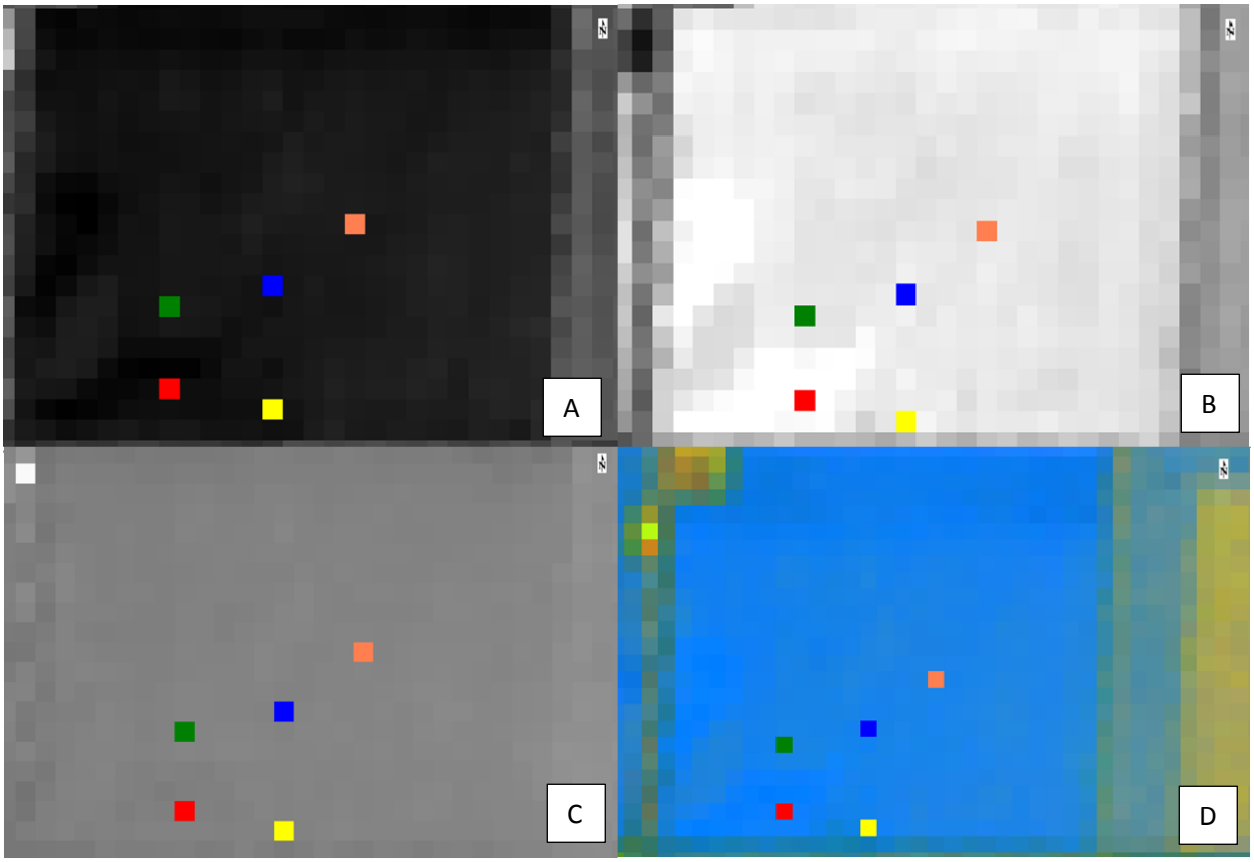

Figure A-2: Study area with Landsat-8 mineral indices applied. (A) Clay mineral index, (B) ferrous minerals index, (C) iron oxide index, and (D) color composite image of all three. Wells are colored pixels in images: well 1: yellow, well 2: red, well 3: green, well 4: blue, well 5: orange.